UNIVERSITÀ DEGLI STUDI DI CAGLIARI

DOTTORATO DI RICERCA IN

SCIENZE MORFOLOGICHE E FUNZIONALI

XXVII CICLO

SETTORE SCIENTIFICO-DISCIPLINARE BIO/16

COORDINATORE: **PROF.SSA VALERIA SOGOS**

EXPLOITATION OF NEW PHARMACOLOGICAL TARGETS FOR NEUROPATHIC PAIN RELIEF

TESI DELLA

DOTT.SSA CRISTINA PICCI

TUTORE

PROF.SSA MARINA QUARTU

ESAME FINALE ANNO ACCADEMICO 2013-2014

TABLE OF CONTENTS

Abstract

Neuropathic pain is a complex chronic condition which affects the somatosensory system, poorly managed with the conventional treatments despite the immense advances in pain treatment strategies. Damage of peripheral nervous system, due to injury or disease, leads to abnormal responses to painful and not-painful stimuli; conventional analgesics can only alleviate pain in acute situation, and finding an effective treatment which can relief chronic neuropathic pain remains still challenging.

Mammalian STOML3, a MEC-2 homologue, is a member of a large family of stomatin proteins characterized by a common stomatin domain, expressed by DRG sensory neurons involved in regulation of mechanosensation, which is required for normal mechanoreceptor function. Previous data revealed that in STOML3 null mice 30-40% of Aδ and Aβ fibers lacked all mechanosensitivity; in addition, tactile behaviors are impaired and symptoms of neuropathic pain in CCI mice are also largely attenuated (Wetzel et al, 2007).

Here I investigated the mechanisms by which STOML3 acts as an important contributor in the neuropathic pain symptoms and I demonstrate that small molecule modulation that both reversibly silence mechanoreceptors in vivo and attenuate touch perception in mice can reverse established neuropathic pain symptoms, making STOML3 a promising novel peripheral target for the treatment of sensory disorders.

Keywords: primary sensory neurons; stomatin-domain proteins; touch; sensory transduction; neuropathic pain; chronic-constriction injury; behavioural assessment; CLARITY method; immunochemistry; molecular biology.

1. Introduction

1.1 Neuropathic Pain

Diabetic neuropathy, viral infections, major surgeries, spinal cord injury, stroke: these are just few examples of a wide range of conditions underlying the etiology of ***neuropathic pain*****,** a complex pathological syndrome which can lead to serious disability and has an important impact on the population (it has been estimated that 8% of Europeans is affected).

As early as childhood, we all have experienced the physiophathological modifications that occur following tissue damage, establishing deep but reversible pain hypersensitivity in inflamed and surrounding tissue in order to assist the wound repair; on the other hand, tissue damage either in peripheral (i.e. peripheral nerves, dorsal root ganglia, dorsal roots) or in central nervous system (i.e. spinal cord, thalamus) might lead to abnormal responses of the body and chronic disorders, which characterize various forms of neuropathies.

From a clinical point of view the occurrence of neuropathic pain is often characterized by *stimulus-independent persistent pain*, a spontaneous syndrome that may depend on both activity of sympathetic nervous system and spontaneous firing of C-fibre nociceptors, or *stimulus-dependent pain*, further sub-classified according to the stimulus that triggers it. Within the latter is comprised one of the key features of neuropathic pain, so-called touch-evoked pain or *allodynia* (Woolf & Mannion, 1999).

The term hyperalgesia is nowadays defined as an increased pain response to a suprathreshold noxious stimulus resulting from an abnormal input processing,

whereas allodynia leads to pain perception on exposure to normally innocuous tactile stimuli; it thus represents a form of pain due to a innocuous stimulus, resulting from low-threshold sensory fiber excitation.

So far, despite the advances in understandings the mechanisms underlying the various disorders following peripheral injuries, no effective treatment has been found yet; some patients may not respond to common therapeutic strategies such as not-steroidal anti inflammatory drugs, or they may develop resistance to opioids. Furthermore, local anesthetics have short-lived effects while antidepressants and anticonvulsants have limited efficacy and too many side effects. Patients may develop even no pain or limited reduction of it after administration of tolerated doses of drug; therefore, there is a need for more effective analgesics and novel strategies for analgesics drug development.

1.2 Mechanisms of peripheral neuropathic pain

1.2.1 Stimulus-independent pain

One of the most dramatic symptoms that characterize peripheral neuropathies is a spontaneous and severe pain experience. Stimulus-independent or ongoing pain is actually very hard to assess in preclinical studies due to the difficulty in its evaluation in animal models; however, physiological and pharmacological changes underlying stimulus independent pain have been well investigated.

Peripheral nerve damage leads to an initial burst of high-frequency discharge followed by ectopic activity generated in the DRGs and neuroma at the site of the lesion (Chen and Devor, 1998; Xie et al., 1995). Spontaneous firing is recorded in both injured and neighbors not-injured fibers, from the early post-lesion period (12h-3days) which lasts over two months paralleling abnormal pain behaviors (Kim, Yoon, & Chung, 1997).

This hyperexcitability has been related to Na+ channel plasticity (Baker & Wood, 2001; Devor, Jänig, & Michaelis, 1994); after nerve injury, Na^+ channels accumulates at the neuroma site and along the axon length, drives to foci of excitability and action potential discharge in injured sensory neurons. Unluckily, conventional treatments with Na^+ channels blockers are not specific and give a wide range of side-effects.

Sympathetic nervous system plays also an important role in spontaneous pain maintainement, due to an over-expression of α-adrenoreceptors and a consequent hypersensitivity to circulating catecholamines. Sympathetic fibers sprouting forming pericellular baskets around the soma of DRGs sensory neurons has also been reported (McLachlan et al., 1993). Moreover, GABAergic tone reduction in the dorsal horn and both GABA and opioid receptors down-regulation enable disinhibition of excitatory impulses with subsequent lowering of peripheral nociceptive thresholds (Gwak et al., 2008), making opiates and GABA-mimic drugs a useful therapeutical approach.

1.2.2 Touch-evoked pain

It has been widely reported that, under normal conditions, the specific stimulation of thin weakly-myelinated Aδ-fibers and unmyelinated C-fibers triggers nociceptive pain, while light touch sensation is selectively carried by low-threshold Aβ-fibers, whose activation normally does not evoke pain.

By contrast, one of the major features of neuropathic pain syndrome is that the activation of low threshold Aβ-fibers, which normally triggers innocuous light touch sensation, is now able to cause intense pain (Costigan, Scholz, & Woolf, 2009; Lewin & Moshourab, 2004; von Hehn, Baron, & Woolf, 2012).

Central sensitization through sustained activation of nociceptors plays a key role in mechanical hyperalgesia; glutamate release following nociceptors activation depolarizes the dorsal horn neurons; inflammatory mediators and neuropeptides such Substance P are also released, extending the depolarization and increasing the intracellular Ca^{2+} concentration, matching the reduction of the GABAergic tone in the spinal cord. Central sensitization causes an enlargement of the peripheral area in

which the stimuli can activate the neurons, increasing of the responses to a supra-threshold input and in making subthreshold inputs reach the threshold and initiate a action potential.

Aβ-fiber-mediated pain may also result from A-*fibre sprouting in lamina II of the spinal cord dorsal horn.* Under normal conditions lamina II only receives nociceptive information; sprouting of A-fibers in lamina II leads to misreading of innocuous stimuli as noxious by the Central Nervous System (CNS) (Woolf et al., 1994).

Moreover, a *phenotype switching* of A-fibers has also been reported after peripheral injury. Calcitonin gene-related peptide (CGRP) and Substance P (SP) play an important role in pain processing and hyperalgesia, and they are normally released by C- and Aδ-fibers. Following peripheral lesion, they have been shown to be down-regulated in medium and small- sized cells but released from large-myelinated Aβ-fibers (Miki et al., 1998); thus, even innocuous stimuli which activate Aβ-fibers might cause release of CGRP and Substance P in the dorsal horn leading to central hyperexcitability.

1.2.3 Spinal glia response at peripheral injury

Microglia, astrocytes and oligodendrocytes represent altogether about 70% of the entire cell population in brain and spinal cord. At spinal level, microglia plays a key role in the pathogenesis of neuropathic pain. Spinal microglia establishes the first noticeable response in spinal cord after several type of peripheral insults. Upon activation, it has been shown to act as a "linker" between the initial injury and the long term neuronal plasticity leading to pain amplification, and the functional and phenotypic pattern of activation strongly depends on the type of peripheral stimulus.
It has been shown that the number of microglial cells and astrocytes increases in spinal dorsal horn ipsilaterally to a peripheral nerve injury (Aldskogius & Kozlova, 1998). After 4h following L5 transection, the microglia activation markers toll-like receptor 4 and cluster determinant 14 mRNA are up-regulated and subsequently decline after 28 days (Tanga, Raghavendra, & DeLeo, 2004). The astrocyte marker

glial fibrillary acidic protein is upregulated as well, starting on postoperative day 4 through day 28 (Tanga et al., 2004).

Upon activation, microglia produces and releases substances including cytokines, prostaglandins, nitric oxide and excitatory amino acids such as glutamate, that act as hyperalgesia mediators. Thus, it has been proposed that microglia is the first immunoeffector cell sensor that, if inhibited before the onset of astrocyte activation, may prevent mechanical hyperalgesia in various models of neuropathy (Tanga et al., 2004). Indeed, selective blockade of glial cells activation prevents and reverses abnormal pain sensitivity: selective inhibition of glial metabolism by fluorocitrate intrathecal administration results in a marked and reversible attenuation of thermal and mechanical hyperalgesia; blockade of CX3C receptors reverses hyperalgesia when applied 5-7 days after sciatic nerve CCI (Milligan et al., 2004). When microglia grown in culture and activated by ATP are injected intrathecally in rats, mechanical hyperalgesia similar to that observed after spinal nerve ligation is induced, while inactive microglia have no effect (Tsuda et al., 2003).

1.3 Models of induced- neuropathy in mice

Development of animal models that reproduce symptoms of human neuropathic pain has been critical in order to elucidate the neurobiological mechanisms underlying the change in the function, chemistry, and structure of neurons in neuropathic pain.
Whereas spontaneous ongoing pain is hard to assess and quantify in preclinical studies due to the technical difficulty in measuring its signs in rodents behavior, abnormal responses to thermal-, chemical- or touch-evoked pain can be well assessed. For this reason, effects of hypothetical analgesic compounds are largely evaluated on their effects in allodynia and hyperalgesia, with minor effort on spontaneous pain.

Chronic constriction Injury of the sciatic nerve (CCI) (Bennett & Xie, 1988) is one of the most frequently animal models used for the study of neuropathic pain molecular mechanism and for the evaluation of pharmacological treatments. This model is based on a unilateral loose ligation of the sciatic nerve enough to occlude but not to arrest the epineural blood flow. However, this causes a near complete loss of large myelinated fibers distal to the ligature in rats (Basbaum, 1991) as a result of direct damage on the afferents.
CCI model produces many of the properties of neuropathic pain in humans; in addiction, it has been demonstrated to be responsive to a wide numbers of compounds which are clinically used as analgesic treatment. CCI leads to a reproducible symptomatic response characterized by decreased threshold in paw withdrawal following thermal, mechanical and chemical stimulation; specific pain behaviors at the injured paw such as shaking or licking; abnormal posture of the injured paw (i. e. toes held together), with an onset within 24 hours until 8-12 weeks. Thus CCI, combined to pain hypersensitivity behavioral tests, provides a reliable system to investigate the effectiveness of potential therapeutic agents.

Peripheral neuropathic pain is produced by multiple etiological factors that initiate a number of diverse mechanisms operating at different sites and at different times; it is unlikely that a single animal model will include the full range of the neuropathic pain mechanisms.

Another model which has been investigated in this work is the *spared nerve injury* (SNI) model (Decosterd and Woolf, 2000), which has been recently developed as an additional animal model of persistent neuropathic pain. It involves a lesion of two of the three terminal branches of the sciatic nerve (tibial and common peroneal nerves) leaving the remaining sural nerve intact. The SNI model differs from the Chung spinal segmental nerve, the Bennett chronic constriction injury and the Seltzer partial sciatic nerve injury models in that the co-mingling of distal intact axons with degenerating axons is restricted, and it permits behavioral testing of the non-injured skin territories adjacent to the denervated areas. The spared nerve injury results in early (< 24h), prolonged (>6 months) and robust behavioral modifications.

1.4 Somatosensory mechanotransduction

Everything we feel around us and our capability to detect the wide variety of stimuli we are every day in contact with is gated by our *somatosensory system*. It enables us to detect and interpret our environment, serving also an essential protective function by mediating fundamental physiological function as the sight, smell, hearing, and *sense of touch and pain*.

Mechanotransduction is the mechanism by which cells convert a specific mechanical stimulus in an electrical signal, letting us even discriminate between different textures of surfaces. As a general mechanism, the detection of the wide range of mechanical and painful stimuli is performed by *primary sensory neurons***,** whose cell bodies are located outside the spinal cord in a swelling called Dorsal Root Ganglia (DRG). Sensory neurons emit a single axon which split in two branches that act as single axons, called distal and proximal processes. The distal process projects to the skin where they form specialized mechanoreceptors that are tuned to detect mechanical forces such as stretch and vibration, turning them in action potential that bypasses the neuron cell body and continue to propagate along the proximal process, until it will be delivered to a second neuron located in the spinal cord; then the signal will follow an ascendant way passing through thalamus and finally it will reach the cerebral cortex for its final interpretation.

1.4.1 Anatomy of mammalian mechanotransduction

Mechanoreceptors act like "gates" which selectively respond to mechanical forces by causing membrane depolarization in the receptive field. Such depolarization let the sensory afferents to transduce sensory stimuli into action potential firing through activation of *mechanotransducer channels* located on sensory nerves endings.

These selective encoding devices are disseminated throughout the body on skin, viscera and tendons. Mammalian cutaneous receptors are morphologically and physiologically so far the best known: *hair follicles* are responsible for light touch perception, *Merkel-complexes* detect skin-stretch, *Pacinian corpuscle* detects vibratory stimuli and *Meissner corpuscle*s respond to dynamic skin deformation. By contrast, *free nerve endings* are not connected to auxiliary structures and only respond to noxious forces.

All this wide and various set of information are detected and transmitted by different arrays of somatosensory afferents, which are usually classified in sub-groups based on axonal diameter and myelin thickness that confers them well defined electrophysiological properties:

- Large-diameter and thick myelinated *Aβ-fibers* are very rapidly conducting fibers and detect innocuous mechanical stimuli (Lewin et al. 2004). They innervate defined mechanoreceptors both in hairy and glabrous skin.
- Medium-diameter and lightly myelinated *Aδ-fibers* are slowly conducting and can either connect to skin hairs with a light-touch detection function, or lose the myelin sheath and innervate the skin as free-ending nociceptors.
- Small-diameter and unmyelinated *C-fibers* nociceptors terminate as free endings in the skin and respond to all types of noxious stimuli in a slow-adapting manner.

The size of the afferents reflects the cell body size of sensory neurons, and mechanosensory signaling relies on specific cellular morphologies. Peripheral sensory fibers, before joining and entering together in the spinal cord via the dorsal root, reach a swelling, called *Dorsal Root Ganglion***,** which hosts cell bodies of primary sensory neurons.

The latter are classified in subpopulations based on their anatomy, neurochemistry and physiology (Lawson et al., 1992). *Large-size* neurons represent about 40% of the entire population, send out myelinated axons that fell in the Aβ-fiber range and receive input from peripheral mechanoreceptors (Sommer, Kazimierczak, & Droz, 1985); *medium-size* neurons give off thin myelinated axons which conduct in the Aδ-fibers range, while *small-size* neurons emit unmyelinated fibers which act as nociceptors (McCarthy & Lawson, 1990).

1.4.2 Physiology of mechanotransduction

How mechanical sensory cells convert mechanical forces in electrical signs in vertebrates and the nature of the transduction molecules involved together with the developmental events that lead to specification of the appropriate sensory neuron sub-types are still matter of study.

Excitatory ion channels are essential in touch reception, but despite genetic screens in *C. elegans* already permitted to identify some of them in invertebrates (Deg/ENaC, TRP channel families), further investigations have to be done in mammalians.

Consistent genetic and molecular evidences lead to propose a *tether model of mechanotransduction*. In this model the ion channel, which represents the "core" of the complex, has been supposed to be "tethered", or anchored by intra- and extracellular domains both to cytosketeton and extracellular structures, to which forces are applied; in this way, deflections of the anchor points lead to a conformation change of the ion channel enhancing its open-status probability.

Although the exact composition of many components of the mechanotransduction machinery is still matter of study, several ion channels have been propose to be involved in touch sensation. Studies in transgenic models recently found novel touchy ion channels called *Piezo family* (Coste et al., 2010) as well as touch modulatory proteins which influence touch sensitivity through a modulatory role such as **STOML3** (Wetzel et al., 2007).

1.4.3 From *C. Elegans* to mammals: discovering molecules involved in touch sensation

The tiny nematode *Caenorhabditis elegans* (*C. Elegans*) has been a powerful tool in studying various aspects of cell development and function.

In the early 80s, Chalfie and Sulston approached touch development by mutational analysis in *C. elegans,* obtaining more than 500 mutations in about 15 genes which result in loss of touch sensation. Most of these genes, called *mec* (from mechanosensory abnormal), encode for proteins that are part of the mechanotransduction machinery (Fig. 1, a).

From these studies came out the first molecular model for eukaryotic mechanosensation:

- Subunits **MEC-4** and **MEC-10** physically interact in assembling the transducing channel, which is the core of the complex;
- The channel extracellular domains are thought to be linked to the extracellular matrix by associating with the **MEC-5** collagene-like molecule and/or **MEC-9**;
- The channel extracellular domains are hypothesized to be linked with the unique 15-protofilaments microtubule (constituted of **MEC-12** α-tubuline and **MEC-7** β-tubulin) by associating with the **stomatin-related peripheral membrane linker protein MEC-2,** which is exclusively expressed by mechanoreceptor neurons and show homology with *stomatin*, an integral membrane protein found in many cell types and involved in the homeostasis of the cell.

Thus, in this model the channel is stretched between two attachment points. The tethering of the channel subunits both to the extracellular matrix and the cytoskeleton confer channel gating tension; mechanical deflections cause the channel opening by changing the conformation of mechanotransduction machinery (Fig. 1).

Since quite a lot of intriguingly touchy genes came from *C. Elegans* genetic screening, subsequent search for orthologs in other species, and of course in mammals, revealed a number of proteins which might be part of mammalian mechanosensory machinery.

In *C. Elegans,* Degenerin (DEG) genes encode for proteins related to the vertebrate epithelial Na+ channels (ENaCs); since mutations in such genes are related to touch

impairments in *C. elegans*, a role in mechanotransduction for the vertebrate homologs has been proposed.

Acid-sensing ion channels ASICs proteins are activated by extracellular protons and mediate pain induced by acidosis; they were proposed to form the ion channel, even though mouse mutants revealed only mild alteration in mechanosensation (Price et al., 2001; Roza et al., 2004).

Piezo proteins have been recently revealed as the mammalian mechanotransduction ion channels (Coste et al., 2010) and Piezo 2 as the major transducer of mechanical forces in mice (Ranade et al., 2014). By virtue of its ability to potently modulate Piezo channels (Poole, Herget, Lapatsina, Ngo, & Lewin, 2014; Wetzel et al., 2007), STOML3, the MEC-2 mammalian orthologous, has been recently demonstrated to be an essential protein in transducting touch sensation.

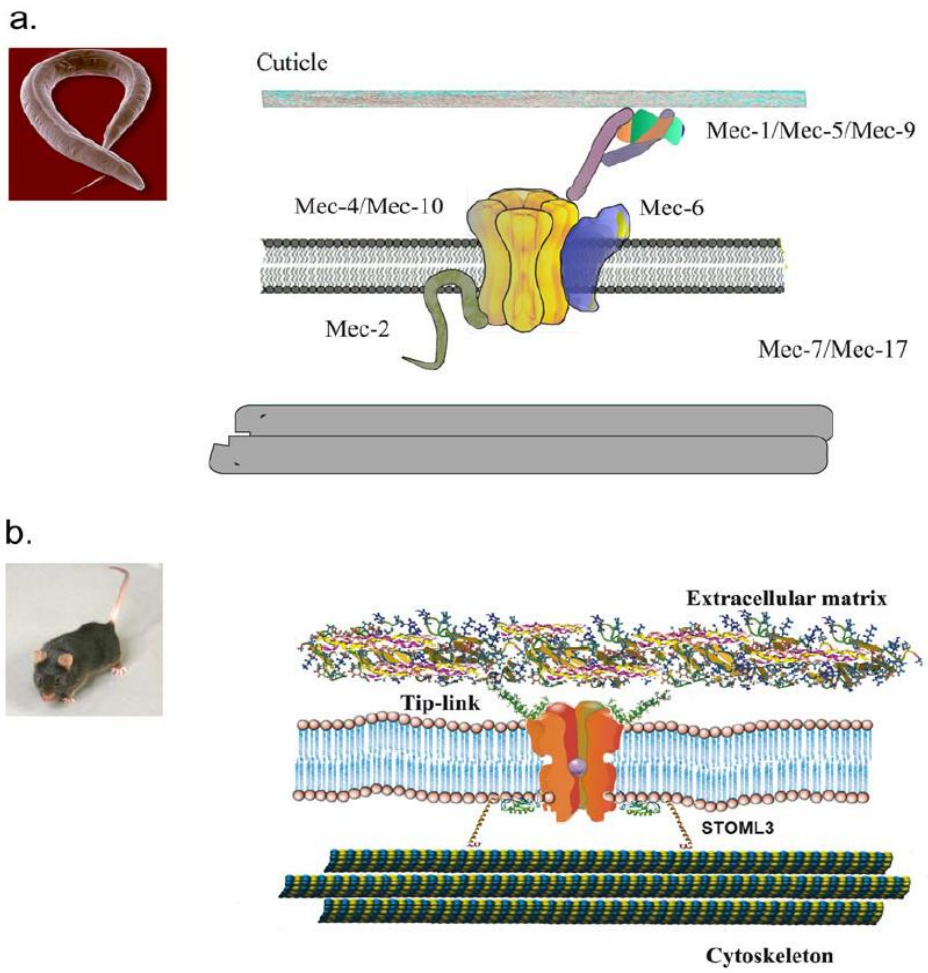

Figure 1. (a) Scheme of *C. elegans* mechanotransducting multiprotein complex formed by MEC proteins. **(b)** A scheme of mechanotransduction machinery in mammals based on the homology of several MEC proteins to mammalian proteins; so far, only STOML3 has been implicated in mechanotransduction.

1.5 Stomatin family of proteins

MEC-2 protein, the best functionally characterized in *C. Elegans*, is 65% identical to stomatin in its central domain, while the N- and C- terminus are not conserved (reviewed in Lapatsina et al., 2012)

Stomatin family of proteins, which include the members Stomatin, STOML1, STOML2, STOML3 and Podocin, share 40-84% of similarity in the sequence of the characteristic stomatin central domain of ~120 residues. They have a similar membrane topology and, with the exception of STOML2 which doesn´t have a hydrophobic domain (Green & Young, 2008), the primary domain organization. All members have different expression patterns and different subcellular distributions.

Stomatin-domain proteins can regulate both ion channels and transporter proteins. The structure of the *stomatin central domain*, which has been found in all kingdoms of life, has been recently solved as an integral membrane protein anchored to the plasma membrane via both a hairpin-like hydrophobic domain and a palmitoylation whose building block is a banana-shape dimer which oligomerizes at the membrane (Brand et al., 2012) (Fig. 2).

Stomatin dimerization is crucial for their ability to modulate both ASIC proteins and mechanosensitive ion channels like Piezo1 and Piezo2 (Brand et al., 2012; Poole et al., 2014). By using a newly developed assay based on elastometric pili, it has been demonstrated that the sensitivity of Piezo channels is exquisitely tuned by STOML3 (Poole et al., 2014). Ongoing work seeks to examinate the precise *in vivo* function of other poorly understood stomatin domain-containing proteins, such as STOML1, for which, by means of advanced cellular imaging techniques in combination with transgenic mouse models, an unexpected role in metabolic disorders has been demonstrated (unpublished data).

1.5.1 Stomatin-like protein 3 (STOML3)

Stomatin family proteins, in particular STOML3, play an essential role in the transduction of mechanical stimuli in vertebrates and invertebrates (reviewed in Lapatsina et al., 2012). STOML3, the mammalian homologue of MEC-2, is an integral membrane protein and an essential accessory subunit for nematode touch receptors (Goodman et al., 2002; O'Hagan, Chalfie, & Goodman, 2005).

Starting from genetic observations of around 15 genes (*mec*) whose function is necessary for touch sensation in *C. Elegans*, mammalian hortologues of *mec* genes were identified, cloned and characterized. Creation of mice with mutant alleles for these genes was crucial to study the in vivo role of the stomatin protein family members in touch sensation and physiology, demonstrating that STOML3 is indeed the MEC-2 hortologous and a crucial subunit in touch sensation (Wetzel et al., 2007)

Loss of mechanically activated currents in cultured DRG neurons is expected to be associated with a loss of mechanosensitivity of sensory fibers in the skin (Wetzel et al., 2007); *Stoml3*$^{-/-}$ mice combined with ad hoc assays as *ex-vivo* skin nerve preparation revealed that ~35% of mechanoreceptors were completely insensitive to mechanical stimuli (Fig. 3). STOML3 mutants have also severe deficits in their ability to detect such textural surfaces with much reduced tactile acuity (Wetzel et al., 2007).

Subjecting wild type and *stoml3*$^{-/-}$ mice to a unilateral sciatic nerve chronic constriction injury (CCI), wild type mice developed a full-blown allodynia; in contrast, *stoml3*$^{-/-}$ mice did not show any hyperalgesia until the third day post-lesion and they developed much milder symptoms. STOML3 null mice are thus largely protected from touch-evoked pain following nerve injury, even though no changes in mechanosensitivity were found in C- fibers (Wetzel et al., 2007). In addition, no impairment was found on the CCI-induced thermal hyperalgesia was found in *stoml3*$^{-/-}$ mice.

Like stomatin, STOML3 is also capable of inhibiting the amplitude of acid-gated currents mediated by ASIC proteins; in the absence of STOML3 in mice, proton gated currents are larger in sensory neurons (Wetzel et al., 2007).

There is a substantial loss of mechanosensitivity in *stoml3*$^{-/-}$ mice in which ~35% of the myelinated fibers lack a mechanosensitive receptive field and this phenotype was

found to be identical in *asic3*$^{-/-}$*:stoml3*$^{-/-}$ mutant mice. Aδ-nociceptors showed much-reduced mechanosensitivity in *asic3*$^{-/-}$*:stoml3*$^{-/-}$ mutant mice compared to *asic3*$^{-/-}$ controls. Loss of stomatin or STOML3 in *asic3*$^{-/-}$ or *asic2*$^{-/-}$ mutant mice markedly exacerbates deficits in the mechanosensitivity of nociceptors without affecting mechanoreceptor function (Moshourab, Wetzel, Martinez-Salgado, & Lewin, 2013).

STOML3 is a powerful positive modulator of Piezo channel mechanosensitivity; structure-function experiments localize the Piezo modulatory activity of STOML3 to the stomatin domain, and higher-order scaffolds are a prerequisite for function (Poole et al., 2014).

These data revealed that STOML-3 is not only necessary for the function of mammalian mechanotransduction complexes but also plays a physiological role in regulating ASIC and Piezo channels in sensory neurons.

Moreover, STOML3 seems to be a promising potential molecular target that directly participates in the transduction of noxious and innocuous mechanical stimuli in sensory neurons; thus, targeting essential mechanotransduction molecules such as STOML3 might provide a novel peripheral means to control sensory disorders.

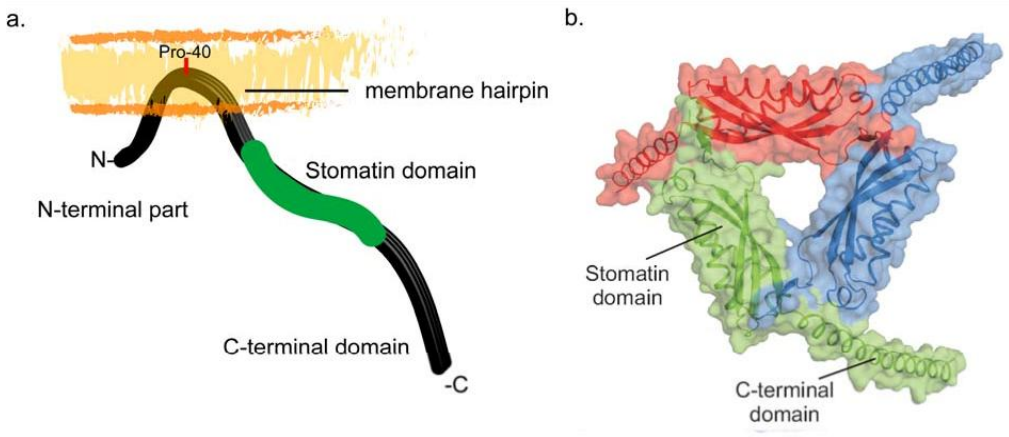

(**from Lapatsina et. Al, European Journal of Cell Biology, 2001**).

Figure 2. **(a)** STOML3 is an integral membrane protein with a single, short and hydrophobic membrane insertion domain followed by the core stomatin domain. A single conserved proline residue in the hydrophobic region is required for the formation of the hairpin structure. Both N-and C-termini are intracellular. **(b)** A homology model of trimeric STOML3, based on the known crystal structure of the *Pyrococcus horikoshii* (ph) stomatin trimer was created using SWISS-MODEL (Brand et al., 2012).

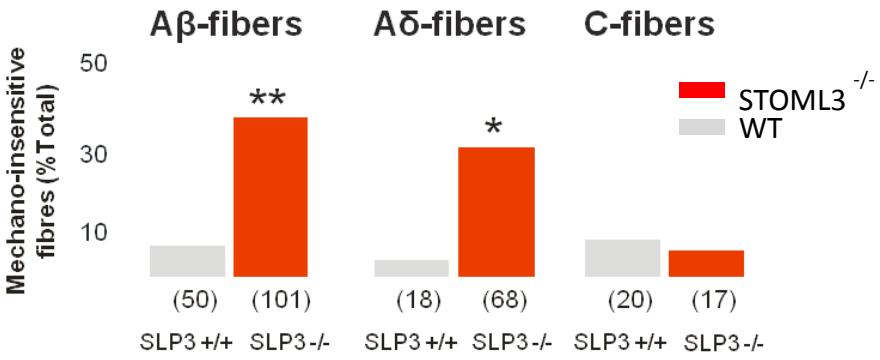

(**from Wetzel et al., Nature, 2007**)

Figure 3. electrophysiological recordings show that about 35% of mechanosensitive fibers do not respond to mechanical stimuli in Stoml3 (SLP3) null mice compared to wild type, while no changes in C-fibers was found.

1.6 Objectives of the study

Neuropathic pain is a debilitating condition for which so far no treatment has been found to be really effective; some patients may not respond to common therapeutic strategies, local anesthetics have short-live effects while antidepressants and anticonvulsants have limited efficacy and too many side effects.

Touch-evoked pain has been assumed to be primarily driven by low threshold mechanoreceptors in humans. STOML3, the mammalian homologue of MEC-2, has been demonstrated to be an essential subunit in modulating mechanotransduction; the intriguingly and unique effect of STOML3 ablation in mechanosensation and the surprising findings that STOML3 null mice are largely protected from touch-evoked pain unraveled a novel interesting role of STOML3 in pathophysiology, making this protein a potential pharmacological target for the treatment of neuropathic pain.

The purpose of this work was primarily focused in understanding the STOML3 role in neuropathic conditions and whether modulation of mechanotransduction by directly acting on STOML3 function might be a novel strategy in the effective treatment of sensory disorders.

In particular, by means of murine models of neuropathic-induced pain combined with behavioral tests for pain assessment, I demonstrate that STOML3 is indeed an important protein whose function is required for conferring hypersensitivity to mechanical stimuli under neuropathic pain conditions *in vivo*. In addition, I provide novel evidence that STOML3 disruption results in the loss of touch-evoked pain symptoms, making the protein a powerful tool for treating sensory disorders resulting from direct damage of afferent fibers.

2. Materials and Methods

2.1 Neuropathic pain mouse models and behavioral pain assessment

2.1.1 Surgery

Chronic constriction injury of the sciatic nerve (CCI). Mice were deeply anesthetized by an induction chamber with 3,5% isoflurane in O_2. After shaving the right hind leg, the shaved area was sterilized with application of 70% isopropyl alcohol. An incision in the skin parallel, but 3-4 mm below the femor, was made, leaving the skin free from the muscles surrounding the incision by cutting through the connective tissue. A retractor was used to widen the gap between the muscles gluteus superficialis and biceps femoris, allowing a clear visualization of the sciatic nerve. Approximately 10 mm of sciatic nerve was gently exposed from the surrounding connective tissue.

Four loosely constrictive silk ligatures (5/0; Catgut GmbH Markneukirchen) with a double knot, 1 mm apart, were placed around the sciatic nerve at the level of the right mid-thigh. Ligatures were the tied until they elicited a brief twitch in the respective hind limb to prevent epidural blood flow. Staples (9 mm) were used to fasten the skin.

Spare nerve injury (SNI). Mice were anesthetized using isoflurane delivered in 100% O2 (Univentor 410 Anaesthesia Unit; Univentor, Malta). After shaving the skin at the mid-tight, a skin and muscle incision was made and the sciatic trifurcation, nerve pieces (2-4 mm) of the sural as well as the common peroneal nerves were removed leaving the tibial nerve intact. Wounds were closed with wound clips before anesthesia was termined.

2.1.2 Assessment of touch-evoked pain: Von-Frey up-down method

Mice were allowed to habituate to the testing apparatus (acrylic chambers 5.5 x 10 cm in size) suspended above a wired mesh grid, one hour before the behavioral testing. Once the mice were resting and not moving, calibrated von-Frey hair monofilaments (Aesthesio® set of 20 monofilaments, Ugo Basile) were applied on the plantar surface of the hind paw in order to deliver target forces from 0.008 to 4 grams increasing in a logarithmic scale. A single stimulus indicated by a slight bending of the stimulus lasted for two seconds unless the mouse withdrew his paw. In order to measure mechanosensitivity the up-and-down method described by Chaplan et al., (1994) was adapted as follows: testing began with a filament delivering a target force of 0.4 grams, and every filament is applied three times. A positive response was noted if the mouse withdrew the paw to all the three filament application, so that the successively smaller filament was presented next. A negative response was noted if the mouse did not respond to at least one out of three applications, and in this case the subsequent larger filament was presented next. Paw withdrawal thresholds were calculated as median of 23 to 30 determined turning points of the particular force stimuli applied to the mouse.

2.1.3 Assessment of thermal hyperalgesia: Hargreaves´s method

Mice were allowed to habituate into a glass chamber (Ugo Basile) one hour before the behavioral testing. Test was performed on the plantar surface of the hind paw by a focused, radiant heat light source (IITC Life Science Inc.).

The light beam was focused to the top of a built-in heating base digitally controlled for consistent temperatures (in this study: 32°C) and created a 4x6mm intense spot on the hind paw of the mouse. The time needed to paw withdrawal in response to a constantly increasing heat stimulus (maximal active intensity: 25% of the light source) with a cut-off of 20 seconds was determined. Heat stimuli were repeated 5 times for each paw with a stimulus interval of 1 minute.

2.1.4 Statistical analysis

All data set were tested for normality. All normally-distributed data sets were compared using a two-tailed Student´s t test. In all cases * indicates $p < 0.05$; ** indicates $p < 0.01$ and *** indicates $p < 0.001$.

2.2 Molecular biology

Tab 1. Kits and enzymes

name	supplier
TURBO DNA-*free*™	Ambion®
SuperScript™ III Reverse Transcriptase	Invitrogen GmbH (Gibco), Karlsruhe, Germany
Universal Mastermix	Roche

Tab 2. Chemicals

name	supplier
Chloroform	Carl Roth GmbH & Co. KG, Karlsruhe, Germany
Ethanol	Carl Roth GmbH & Co. KG, Karlsruhe, Germany
Isopropanol	Carl Roth GmbH & Co. KG, Karlsruhe, Germany
Glycogen	Invitrogen GmbH (Gibco), Karlsruhe, Germany
Trizol	Invitrogen GmbH (Gibco), Karlsruhe, Germany
OligodT	Invitrogen GmbH (Gibco), Karlsruhe, Germany
Random nonamers	Invitrogen GmbH (Gibco), Karlsruhe, Germany
dNTPs	Invitrogen GmbH (Gibco), Karlsruhe, Germany
5X First-Strand Buffer	Invitrogen GmbH (Gibco), Karlsruhe, Germany
DTT	Invitrogen GmbH (Gibco), Karlsruhe, Germany

10X buffer	Invitrogen GmbH (Gibco), Karlsruhe, Germany
$MgCl_2$	Invitrogen GmbH (Gibco), Karlsruhe, Germany
Taq Polimerase	Invitrogen GmbH (Gibco), Karlsruhe, Germany
MasterMix	Invitrogen GmbH (Gibco), Karlsruhe, Germany
Agarose	Invitrogen GmbH (Gibco), Karlsruhe, Germany

2.2.1 Genotyping

Stoml3$^{-/-}$ mice genotyping was carried out by polymerase chain reaction amplification with genomic DNA isolated from mice tail biopsies. The total reaction volume was 20 µl including the DNA sample. The reaction buffer was made as follows:

Standard PCR mic for Taq polymerase	**Cycling protocol**
2 µl 10X buffer	94°C 7 min
1 µl MgCl2	60°C 35 sec
0.4 µl dNTPs	72°C 2 min
0.2 µl primer 3´	94°C 30 sec
0.2 µl primer 5´	60°C 35 sec
0.2 µl Taq polymerase	72°C 2 min, 30 cycles

DNA samples were separated on 1% agarose gel in the EasyCast™ gel system (Owl Thermoscientific). Gel was prepared by microwaving the appropriated amount of

agarose powder in 1X SB buffer. 0.01% of Ethidium Bromide was added to the pre-cooled agarose solution and the gel was poured into the gel slides and allowed to polymerize. DNA samples were mixed with 6X loading dye and ~500 ng DNA were added per gel pocket. The Smart DNA ladder (Eurogen) was used as a DNA-size marker. Electrophoresis was carried out at 70-120 V for 15-25 min and gels were afterward analyzed using the Safe Imager™ blue light (Invitrogen).

2.2.2 Extraction of total RNA from tissue and cells

Lumbar DRGs (L4-5-6) and olfactory bulb were dissected and immediately transferred in 800 µl of Trizol reagent containing 200 µg glycogen (final concentration 250µg/ml) followed by homogenization by power homogenization. Samples were placed 5 minutes at room temperature, and 160µl of chloroform were added afterwards. After vigorous vortexing for 30 seconds, samples were incubated for 3 minutes on the bench. To separate total RNA, samples were centrifuged for 10 minutes at 12000g, 4°C, and the upper acqueous phase containing RNA was transferred into a fresh tube. For RNA precipitation 400 µl of ice-isopropanol were added, and samples were incubated at -20°C overnight. The day after, RNA was pellet by centrifugation at maximum speed 15 minutes at room temperature. After supernatant was decanted, RNA pellet was washed in 200 µl of 70% ethanol and spinned again at maximum speed. The washing phase was repeated or 3 times. Supernatant was decanted without disturbing the pellet; RNA was air-dried and the pellet was resolubilized in 30 µl RNAse-free deionized water.
Tissue culture cells were extensively mixed with TRIZOL with no homogenization step before chloroform addition; the RNA then extracted as described before.

2.2.3 DNA cleaning

DNA was cleaned out from RNA as follows: 0.1 volume of 10X TURBO DNase buffer and 1 µl Turbo DNase were added to the RNA. After mixing gently, the samples were incubated at 37°C for 20-30 minutes.

0.1 volume of DNase Inactivation reagent was added and after mixing samples were incubate 5 min at room temperature, flicking the tube occasionally during incubation period to redisperse the Dnase Inactivation Reagent.
Samples were centrifuged at 10000g for 1.5 min to pellet the DNase Inactivation Reagent, and the cleaned RNA was transferred to a fresh tube.
The quantity and purity of RNA were assessed using a NanoDrop 2000 UV-Vis spectrophotometer (Thermo Scientific).

2.2.4 cDNA synthesis

1.5-2 µg of RNA were used for cDNA synthesis. In a fresh sterilized 0.2 ml tube the following reagents were added:

- 1µl of oligo(dT)20 or 50-250 ng of random primers;
- Total RNA
- 1 µl 10 mM dNTP Mix (10 mM each sATP, dGTP, dCTP and dTTP at neutral pH)
- Sterile, distilled water to 13 µl

The reaction was placed at 65°C for 5 min and incubate on ice for at least 1 min immediately afterwards. After collecting the contents of the tube by brief centrifugation, the following reagents were added:

- 1 µl 5X First-Strand Buffer
- 1 µl 0.1 M DTT
- 1 µl of Superscript® III Retrotranscriptase

After mixing gently by pipetting up and down, samples were incubated at 50°C for 60 min and 70°C for 15 min.

2.2.5 Quantitative Real-Time PCR

The PCR was performed in an ABI PRISM® 7900HT (Applied Biosystem) detection system. Reaction for quantitative real-time PCR using TaqMan detection was modified as follows:

- 3,5 µl of sterile, deionized water
- 0.2 µl forward primer
- 0.2 µl reverse primer
- 0.1 µl probe
- 5 µl MasterMix

The reactions were performed in a 384-well plate capped with MicroAmp optical caps; after putting 9 µl of reaction mix in each well, 1 µl of cDNA was added. Absolute copy number was determined referring to a standard curve which was created by using serially diluted cDNA containing plasmid. Each sample was performed in triplicate; data are presented as mean of number of copies for 1500 ng of total RNA ± S.E.M.

2.3 Histology

Tab 4. Chemicals

name	supplier
Rompun ® (2% Xylazin)	Bayer Vital GmbH, Leverkusen, Germany
Ketamine(10%)	WDT eG, Garbsen, Germany
PBS	Invitrogen GmbH (Gibco), Karlsruhe, Germany
Glutharaldehyde	Sigma-Aldrich Chemie GmbH, Schnelldorf, Germany
X-Gal(bromo-chloro-indolylgalactopyranoside)	Carl Roth GmbH & Co. KG, Karlsruhe, Germany
Sucrose	Sigma-Aldrich Chemie GmbH, Schnelldorf, Germany
OCT	Sakura Finetek, Zoeterwoude, Netherlands
Aqua Polymount	Polisciences, Inc.
Paraformaldehyde	Sigma-Aldrich Chemie GmbH, Schnelldorf, Germany
NaOH	Sigma-Aldrich Chemie GmbH, Schnelldorf, Germany
Triton X-100	Sigma-Aldrich Chemie GmbH, Schnelldorf, Germany
MgCl2 (50 mM)	Invitrogen GmbH, Karlsruhe, Germany
Sodium chloride	Carl Roth GmbH & Co. KG, Karlsruhe, Germany
Nonidet P-40	Sigma-Aldrich Chemie GmbH, Schnelldorf, Germany
Na deoxycholate	Sigma-Aldrich Chemie GmbH, Schnelldorf, Germany
Dimethylformamide	Sigma-Aldrich Chemie GmbH, Schnelldorf, Germany

Tab 5. Buffers

name	composition
0.5% Glutaraldehyde	0.5% Glutaraldehyde, 2 mM MgCl2, 1.25mM EGTA in PBS. pH-7.4
4% PAF	4% Paraformaldehyde, 2 mM MgCl2, 1.25mM EGTA in PBS. pH 7.2-7.4
10X PBS	80g/l NaCl, 2g/l KH2PO4, 2g/l KCl, 21.6g/l Na2HPO4•7H2O
X-Gal reaction buffer	35 mM K4[Fe(CN)6]•3H2O, 35 mM K3[Fe(CN)6], 2mM MgCl2, 0.02% Nonidet P-40, 0.01% Na deoxycholate, 10mg/ml X-gal in dimethylformamide in PBS

2.3.1 *Stoml3*^{LacZ} knock-in mice

In our hands no commercial or custom-made antibodies against STOML3 were available and reliable for specific detection of endogenous STOML3 in DRG neurons. Bacterial β-galactosidase gene (*Lac-Z*) is a powerful tool to detect the *cis*-acting regulatory sequence activity. Therefore, we focused on the study of the STOML3 promoter expression pattern by using an unpublished knock-in mice in which a β-galactosidase cassette with a nuclear localization signal (NLS) was insert with the start codon of STOML3 gene (Fig. 4).

Once introduced under the promoter of the gene of interest, the endogenous expression pattern and the time point in development when the gene is initially expressed can be detected with an enzymatic reaction.

In *Stoml3*^{LacZ} mice used for this study, the first exon of the gene was replaced with a β-galactosidase coding sequence. The gene promoter and regulatory elements were preserved (Fig. 4).

2.3.2 Animal perfusion fixation

Before the perfusion mice were anaesthetized with a mixture of Rompun + Ketavet. 0.02 ml of Rompun (20 mg/ml Xylazine) and 0.1 ml of Ketavet (100 mg/ml Ketavet) were made in 0.4 ml of PBS, and the dose of 0.02 ml/g was injected intraperitoneally. Surgical-plane anaesthesia was assured by the absence of toe-pinch evoked reflexes.
The thoracic cavity was opened by cutting the diaphragm from one lateral aspect to the other lateral aspect. Both lateral aspects of the rib cage were in a caudal to rostral direction up to the second rib and folded-back to expose the thoracic organs. The right atrial chamber was lacerated with scissors while the 25G perfusion needle attached to the saline syringe was carefully inserted into the left ventricular chamber of the hearth. Mice were perfused with ice-cold PBS until liver blanching, followed by 4% PFA or 0,5% glutaraldehyde perfusion for 20 min.
At the completion of the perfusion, lumbar DRGs, spinal cord, olfactory bulb and sciatic nerve, aimed for X-gal, were dissected out, post-fixed for 30 min in 4% glutharaldehyde and dehydrated in 30% sucrose at 4°C overnight.

2.3.3 Detection of *β-gal* activity

Dehydrated tissue samples were embedded in O.C.T. Tissue-Tek, frozen on dry-ice and placed at -80°C prior to use. For histochemical staining, glutaraldheyde fixed tissues were frozen and sectioned with a cryostat (Leica CM3050S), mounted on slides and allowed to dry at room temperature. The thickness of sections varied with the tissue type.
Before the staining, slides were rinsed several times in 1XPBS on ice. Fresh X-Gal buffer was prepared for every experiment. Slides were placed into a histochemical chamber and incubated in X-gal buffer (1mg/ml) at 37°C; the time was dependent on the tissue time, generally 24 hours were requested for DRGs.
Following the staining, slices were intensively washed several times in 1XPBS until the solution no longer turned yellow and cover-slipped with AquaPolymount, and then observed in Zeiss Axiovert 135 by Zen software.

2.3.4 Morphometry

Morphometric analysis was performed on DRG neuronal cell profiles in digital images captured with a 20X objective magnification from 6 mice both naïve and neuropathic, respectively. The tissue slices were separated by at least 30 μm. Image J software was used to manually trace the outlines of cells in order to obtain cell areas, which when then converted in diameter using Excel. Histograms of frequency distribution were plotted using GraphPad Prism.

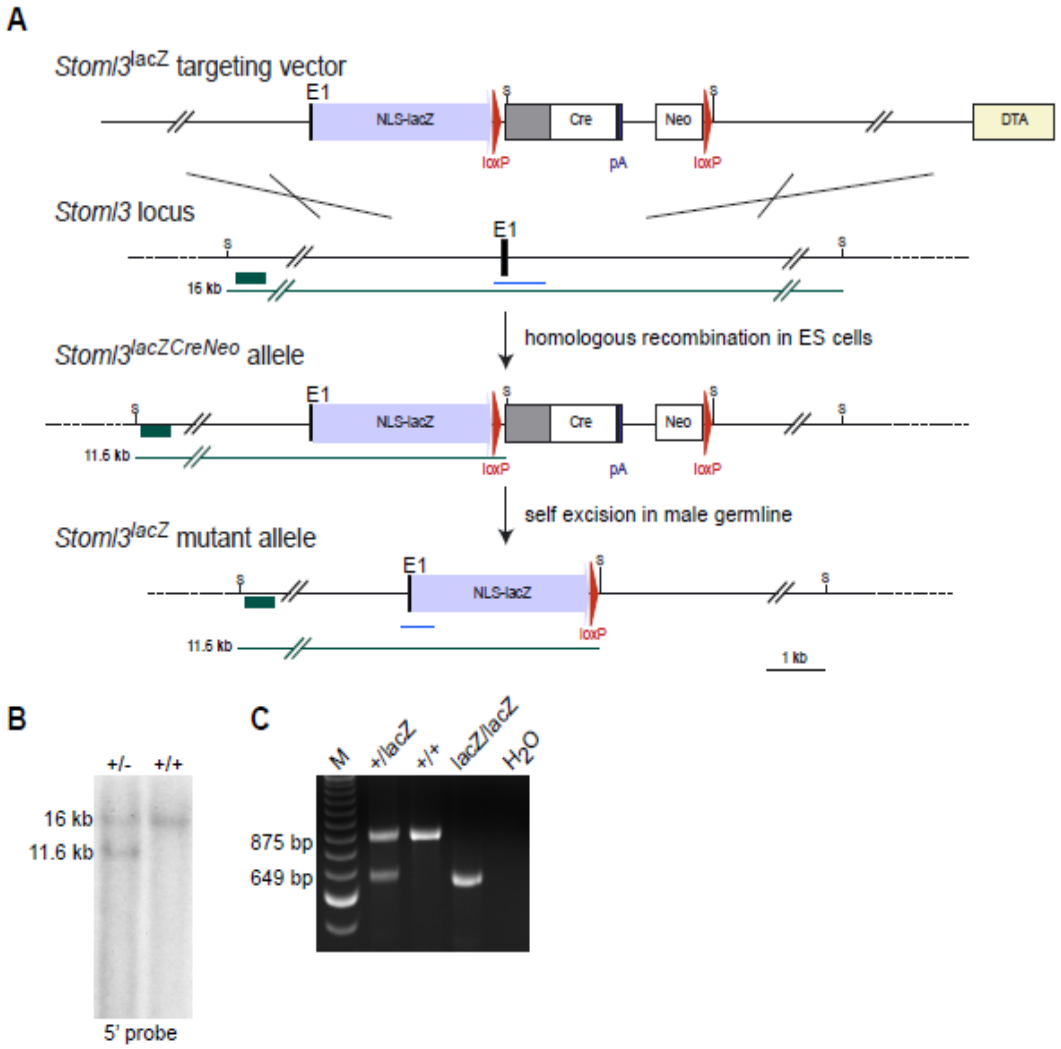

Figure 4. (a) Schematic representation of the linearised targeting vector, the wild type *Stoml3* locus, and the mutated *Stoml3*^{LacZ} allele before and after removal of the self excision neomicyne (cre, neo) cassette. A 12 kb genomic region of *Stoml3* locus containing exon 1 (black) NLS-LacZ (blue) DTA (yellow) the self excision neomycine cassette, loxP (red arrowhead) and SpeI (S) restriction sites are depicted. Green lines indicate the predicted fragments sizes obtained after SpeI digestion of Genomic DNA. A green bar shows the 5' probe used for southern blot analysis shown in **(b)**, blue lines indicate the predicted fragment sized obtaining by genotyping the tail genomic DNA as shown in **(c).**

2.4 CLARITY

2.4.1 McGreen mice

Mice were kindly provided by Helmut Kettenmann laboratory. In *Cx3cr1*$^{GFP/GFP}$ mice (McGreen mice) that were used for this study, both copies of the *Cx3cr1* gene have been replaced by the enhanced Green Fluorescent Protein (**eGFP**) reporter gene. Homozygous mice for the *Cx3cr1* gene are fertile, normal in size and do not display physical or behavioral abnormalities.

Tab. 6 Chemicals

name	supplier
FocusClear	Cell Explorer Labs CO
Va-044 initiator	Wako Pure Chemical industries, Ltd
Bisacrylamide	BIO-RAD
Acrylamide	BIO-RAD
Boric Acid	Biozym
SDS	Carl Roth GmbH & Co. KG, Karlsruhe, Germany
NaOH	Carl Roth GmbH & Co. KG, Karlsruhe, Germany

Tab. 7 Hydrogel monomer solution

Ingredient	Final concentration
Acrylamide 40%	**4%**
Bisacrylamide 2%	**0.05%**
VA-044 initiator	**0.25%**
10X PBS	**1X**
PFA 16%	**4%**
dH2O	**to 400 ml**

Tab 8. Clearing solution

Ingredient	Final concentration
Boric Acid	**200mM**
Sodium Dodecyl Sulfate	**4%**
NaOH to pH 8.5	**-**
dH2O	**To 10L**

2.4.2 Hydrogel and Clearing solution preparation

Ingredients showed in tab1 were mixed under the hood with special attention to temperature and safety precautions, keeping all components in ice to avoid polymerization. After 40 ml were distributed into 50 ml conical tubes on ice, tubes were sealed tightly and stored at -20°C until they were ready for use.

Clearing Solution was made under a hood with special attention to safety precautions. Ingredients in tab.2 were combined at room temperature while stirring, and NaOH was added until the pH has reached 8.5; the solution was stored at room temperature.

2.4.3 Transcardial perfusion with hydrogel solution

Frozen hydrogel monomer solution was thawed and mixed gently prior to perfusing, making sure there were not precipitates or bubbles in the solution.
Adult mice were deeply anaesthetized with Rompun Xylazine plus Ketamine in PBS and perfused first with 20 ml of ice-cold 1x PBS and then with 20 ml of ice-cold hydrogel solution, maintaining a rate of perfusion of about 2 minutes for the 20 ml of each solution.
Spinal cord was then dissected out and immediately placed in 20 ml of cold hydrogel solution in a 50 ml conical tube, covered in aluminum foil and incubated at 4°C for 24 hours to allow for further diffusion of the hydrogel solution into the tissue.

2.4.4 Hydrogel tissue embedding

50 ml conical tube containing the tissue was placed in a desiccation chamber under the fume hood. Cap was opened sufficiently to allow gas exchange; the chamber was degassed for 10 minutes through a vacuum pump, and then the chamber was filled with argon gas for other 10 minutes.
The chamber was then opened sufficiently to reach the tubes in order to tightly close the sample tube, carefully minimizing exposure to air.
Tubes were submerged in 37° water bath for 3 hours until solution had polymerized.
After 3 h, in a fume hood, the embedded tissue was extracted from the gel, and extra gel pieces were removed with gloved fingers.
The samples were washed with 50 ml of clearing solution for 24 hours at room temperature to dialyze out extra PFA or monomer, and then they were washed 2 more times for 24 hours each, to further reduce residual PFA, initiator or monomer.

2.4.5 Electrophoretic tissue clearing

Tissues were placed in the electrophoretic chamber, putting one tissue in each chamber. Clearing solution was circulated through the chamber, with 25V applied across the tissue at 37 degrees for several days until the tissue became transparent. Alternatively, passive clearing was also made; tissue was in 37°C room while shaking for at least 4 weeks, until the tissue turned transparent.
After several days, samples were washed with PBS-T twice for 24 hours each.

2.4.6 Preparing the sample for imaging

Samples were incubated in FocusClear for 2 days protected from light. Samples were placed in a ad-hoc space built attaching a press-to-seal Silicone isolator in WillCo-Dish°, surrounded with enough FocusClear to surround the tissue, ensuring not to introduce any bubble. Once the chamber was entirely filled with FocusClear, the chamber was sealed with a glass coverslip. Confocal images were taken with Zeiss Axio Observer z1 microscope using Zen imaging software (Zeiss).

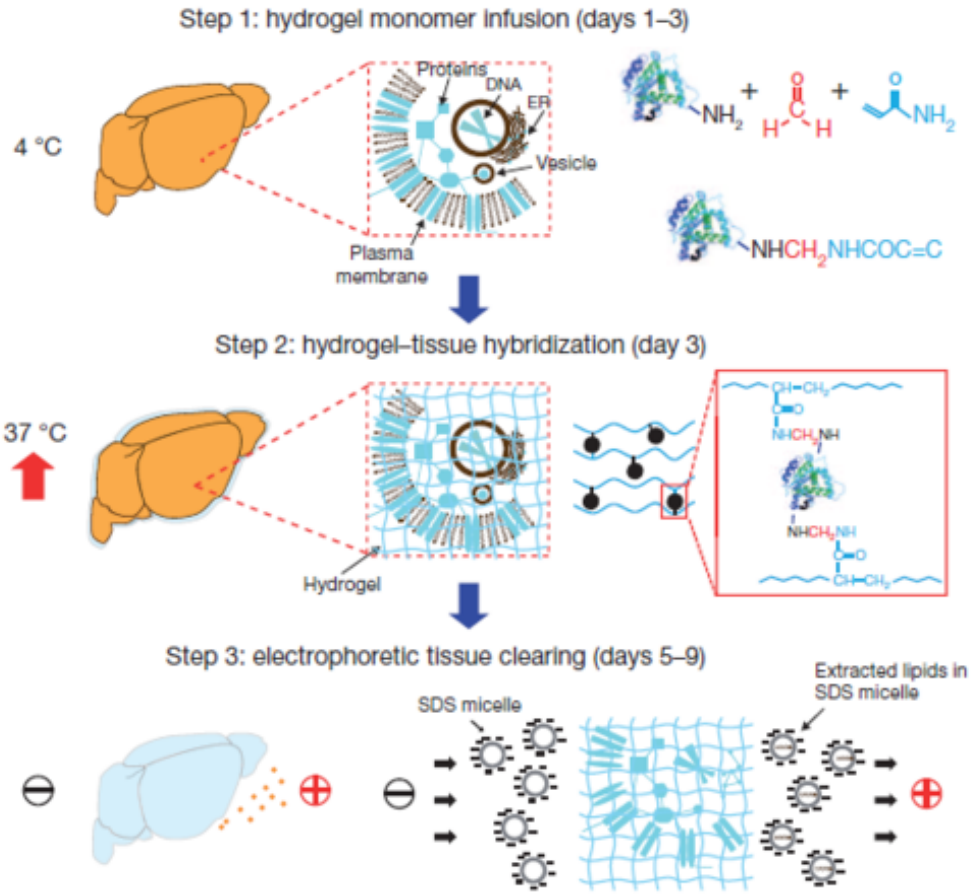

(From Chung et al., Nature, 2013)

Figure 5. (a) Tissue is cross-linked with formaldehyde (red) in presence of hydrogel monomers (blue) covalently linking tissue elements to monomers that are then polymerized into a hydrogel mesh. Electric field applied across the sample in ionic detergent actively transport micelles into, and lipids out of the tissue, leaving fine structures and crosslinked molecules in place. **(b)** A clarified mouse spinal cord.

3. Results

3.1 Characterization of STOML3 *in vivo* expression pattern

STOML3 was first identified as an olfactory epithelium specific protein, whose role was consistent with the assembly, translocation, or function of the odorant transduction complex in olfactory neurons (Kobayakawa et al., 2002). Because of the selective localization of the Stoml3 mRNA to the olfactory cells, early studies suggested a specific role for the protein in the unique transduction pathway of olfactory neurons (Goldstein et al., 2003). STOML3 has an homologue in *C. Elegans*, MEC-2, which acts as a linker between MEC-4/MEC-10 ion channel and the cytoskeleton; its essential role in mechanotransduction was then demonstrated (Wetzel et al., 2007)

To characterize the *in-vivo* expression pattern of STOML3, I investigated olfactory bulb, the whole spinal cord and lumbar DRGs of a reporter *Stoml3*^{LacZ} mouse line, in which a *β-galactosidase* cassette with a nuclear localization signal (NLS) was inserted in place of the first exon of the Stoml3 gene under the control of Stoml3 promoter. This assay allows detecting *β-galactosidase* activity, which reflects the endogenous activity of the Stoml3 promoter, and thus sensory neurons that normally express STOML3 by means of a blu-violet spot located next to the nucleus that can be seen under a bright-field microscope. However, due to the nuclear localization of the signal sequence, X-gal staining does not predict the subcellular localization of the gene.

In general, X-gal staining in *Stoml3*^{lacZ} adult mice gave a robust signal only in olfactory bulb, whereas it gave a quite modest staining in spinal cord and lumbar DRGs due to a low expression of the gene.

Olfactory bulb. It has a laminar architecture with interneuron cell bodies lying around and beneath the outer stratum, called the *glomerular layer*, that receives direct input from olfactory nerves. An external *plexiform layer*, containing astrocytes and interneurons, links the *glomerular layer* with the more internal *mitral layer* which projects to olfactory cortex. In the center of the olfactory bulb, lies the *granule cell layer*.

X-gal assay revealed a robust STOML3 expression in the glomerular layer, in which separate glomeruli developed a pronounced staining, and a moderate expression in the mitral layer (Fig. 5 a, b).

Spinal cord. Transverse sections of spinal cord from *Stoml3*^{lacZ} mice showed a strong signal in cells lining the central canal, with rare additional cells modest staining all over the gray matter, revealing a restricted pattern with a prominent staining in certain cells in ependyma (Fig. 5 c, d).

Lumbar DRGs. The evidence that STOML3 null mice show a loss of mechanosensitivity in about 35% of skin mechanoreceptors (Wetzel et al., 2007) lead to investigate whether it can be due to a restricted expression of STOML3 by a distinct neuronal subpopulation; L4-L6 lumbar DRG sections were thus analyzed. Interestingly, only about 35-40% of DRG neurons developed an enzymatic reaction and expressed *β-gal* activity*;* in addition, only large- and medium-sized neurons developed a visible staining, as morphometrical analysis confirmed (Fig. 6 a, b, c). It can be thus assumed that STOML3 expression is restricted to a sub-population of mechanoreceptor sensory neurons.

Stoml3 gene expression with ageing. The observation that *Stoml3*$^{-/-}$ mice are largely protected from mechanical neuropathic symptoms led to hypothesize that STOML3 could be considered an important factor in the onset of sensory disorders. A decline in the main sensory modalities, including touch sensation is widely reported to occur with ageing. A decrease of Stoml3 gene expression would be then related to loss of mechanosensitivity, as well as in raising the sensitivity to brush field under certain neuropathic conditions. Therefore, I asked whether STOML3 would have a

role in decreasing touch sensation with advancing age. Quantitative real-time PCR (qPCR) of lumbar L4-6 DRGs from wild type mice revealed a significant down-regulation of Stoml3 mRNA copy number in 12 weeks old compared to 42 weeks old mice (Fig. 6 d), suggesting a role for STOML3 in the decline of mechanosensitivity with advancing age. Further electrophysiological experiments should be carried out in old mice in order to investigate changes in mechanical sensitivity.

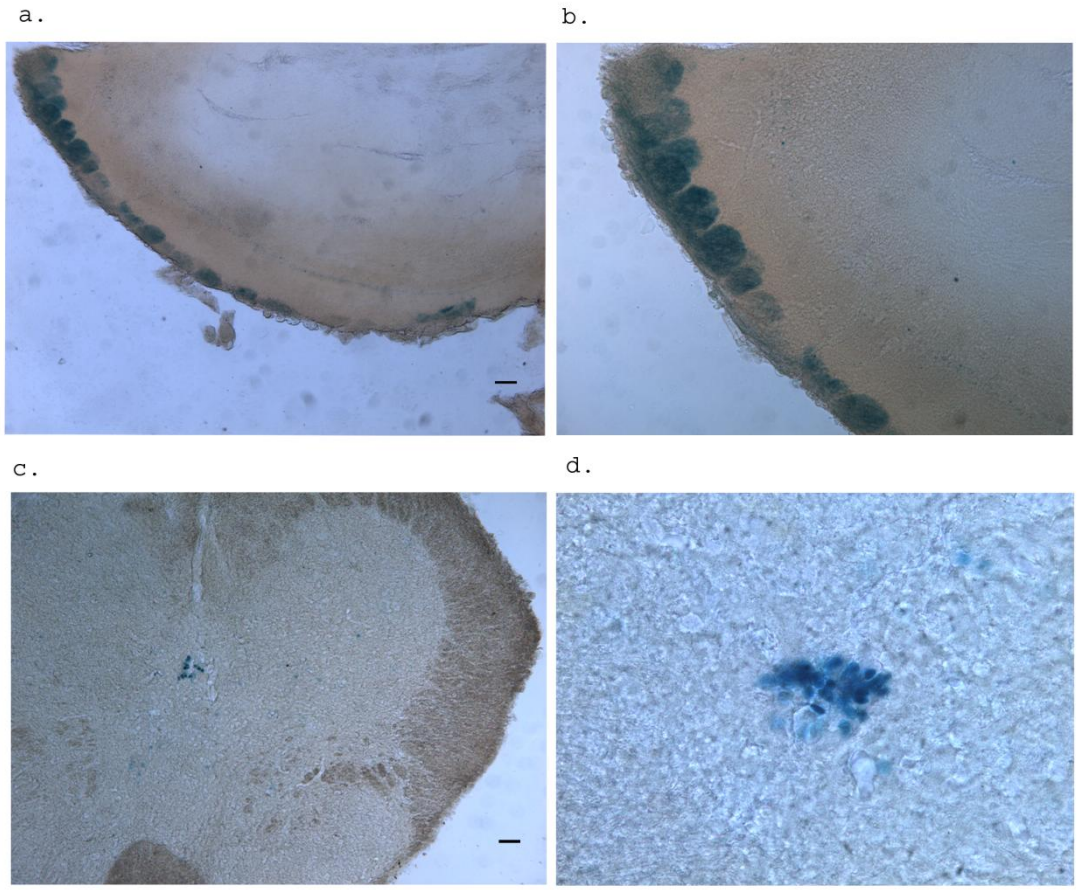

Figure 6. (a) Transverse section of Olfactory Bulb. **(b)** Magnified region (20X) of the glomerular layer, separate glomeruli develop X-gal coloration.
(c) Transverse sections of the lumbar region of Spinal Cord; STOML3 endogenous expression is restricted to cells surrounding the central canal **(d)** Magnified region (40X) of the central canal. Bar – 20 μm

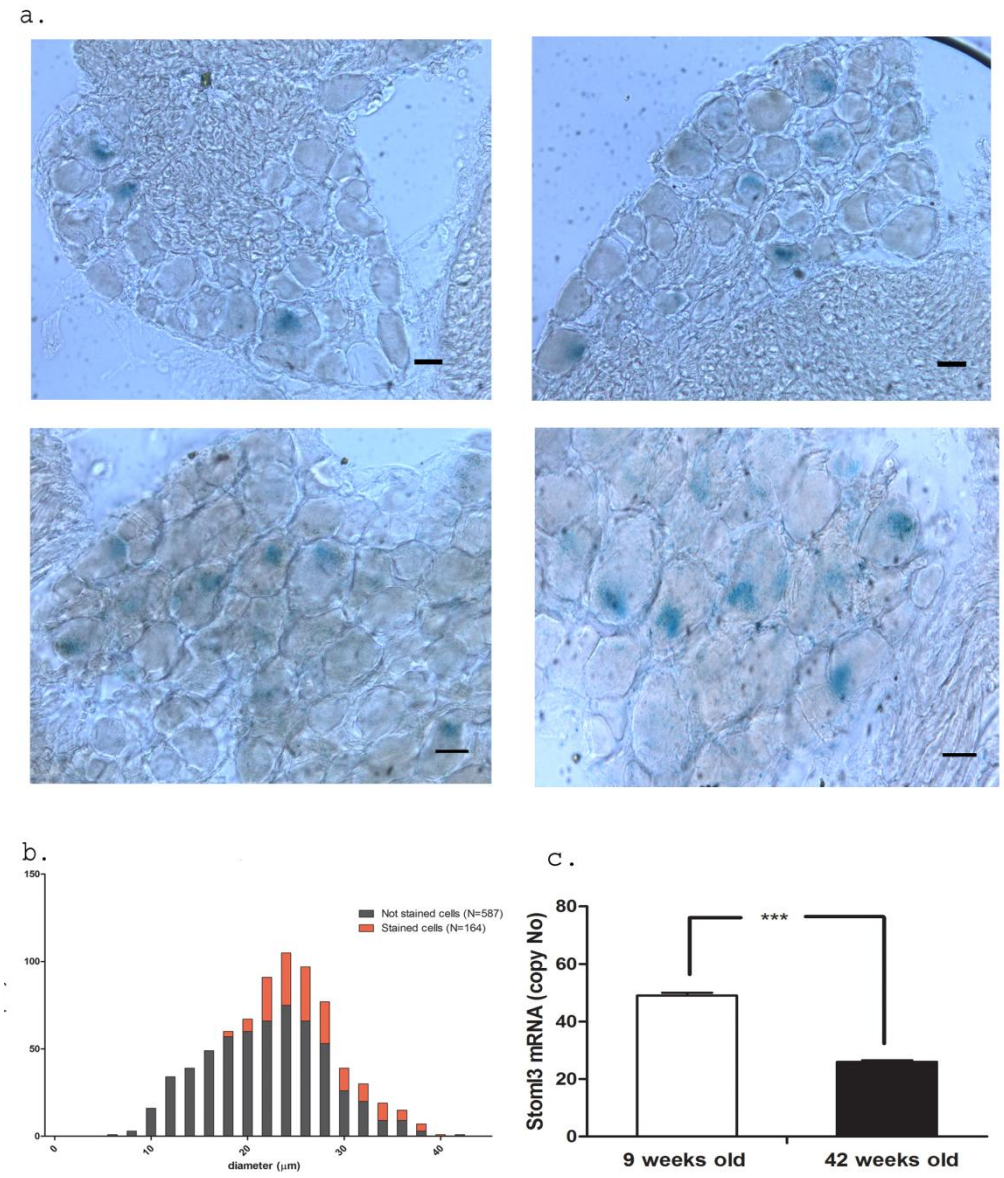

Figure 7. (a) Stoml3 endogenous expression in lumbar DRGs. Bar – 20micron. **(b)** X-gal positive staining is restricted to medium and large sized-neurons**.** Quantitative real-time PCR (qPCR) revealed a significant down-regulation of Stoml3 mRNA copy number in 12 weeks old mice compared to 42 weeks old mice (***p<0.001; Student T- test; error bars indicate s.e.m.).

3.2 Characterization of CCI mice

3.2.1 Mechanical and Behavioral assessment

STOML3 is a membrane-associate protein expressed in sensory neurons and selectively associated to skin mechanoreceptors required for normal touch sensation in mouse. Electrophysiological recordings in STOML3 null mice indicate that a large proportion (about 45%) of rapidly adapting mechanoreceptors (RAM) fibers were unresponsive to very fast movements; the stimulus response in slowly adapting mechanoreceptors (SAM) was mildly but significantly impaired; the remaining RAM fibers and the D-hair fibers had normal mechanosensitivity. In addition, Aδ-fiber mechano-nociceptors and C-fibre nociceptors both displayed normal mechanosensitivity in *Stoml3* mutant mice (Wetzel et al., 2007).

Under neuropathic conditions, stimulation of low-threshold mechanoreceptors by brushing the skin can lead to intense pain in humans and animals. In order to establish the presence of mechanical allodynia, C57BL/6N wild type and *Stoml3*$^{-/-}$ mice were both subjected to a unilateral sciatic nerve chronic constriction injury (CCI).

The complete absence of Stoml3 mRNA expression in *Stoml3*$^{-/-}$ animals was confirmed by qPCR. Mechanical allodynia was assessed with Von Frey hairs using the Von Frey adapted *up-down* method, while thermal hyperalgesia symptoms were evaluated by measuring paw withdrawal latency in seconds by using Hargreaves method. Baseline withdrawal thresholds did not differ in wild type and *Stoml3*$^{-/-}$ mice before the surgery. After being subjected to CCI, wild type mice developed within a few days a full-blown allodynia with mechanical thresholds for paw withdrawal decreasing from 1.2 g to 0.04 g until the end of the measurements; thermal hyperalgesia symptoms were also fully developed with the withdrawal latency dropping down from 5 seconds to 3 seconds (Fig. 7 a, b). In contrast, STOML3 null mice did not show any mechanical hyperalgesia until the third day of lesion, and mechanical threshold decreased to just 0.6 g until the end of the observation period. Thermal withdrawal thresholds did no differ between control and STOML3 null mice

(Fig. 7 a, b); after 15 days both seemed to recover, as the paw withdrawal latency started to go up again (data not shown).

3.2.2 Spinal glia response in CCI mice

There is a rapidly growing body of evidence indicating that spinal microglia signalling plays a key role in the pathogenesis of neuropathic pain; glia inhibitors or glia modifying compounds can alter pain sensitivity, making glial cells an interesting target for neuropathic pain treatment.

Clear, Lipid-exchanged, Acrylamide-hybridized Rigid, Imaging/immunostaining compatible, Tissue hYdrogel, (CLARITY), is a novel imaging technique (Chung et al., 2013) that allows to transform intact biological structures into a hybrid form in which tissue components are removed and replaced with exogenous elements for increased accessibility and functionality. This technique makes tissues see-through without destroy the tissue structure. When accompanied with antibody labeling, Clarity provides detailed pictures of fine structure, proteins and nucleic acids. I applied this method in transgenic McGreen mice, generously provided by Prof. Helmut Kettenman, in which the Cx3cr1 gene has been replaced by the enhanced Green Fluorescent Protein (eGFP) reporter gene, so that microglia can be directly visualized as fluorescent elements without using antibodies.

Adult McGreen mice were subjected to CCI as described before. After assessing development of the neuropathic symptoms, spinal cord of naïve and CCI McGreen mice were dissected out and processed for CLARITY technique; microglia is here identified by means of CX3CR1 expression in CX3CR1-GFP mice.

Z-stack confocal images from the dorsal to the ventral side of the lumbar spinal cord showed detailed pictures of microglia distribution. 3-D stacks from naïve mice displayed that microglia distribution do not differ between spinal cord antimeres (Fig. 8 a, b, c); in CCI mice microglia appears to migrate and accumulate at focal sites of injury in the area where damaged axons project to. Nerve injury inducted-microglial reaction is remarkable in the ipsilateral side of spinal cord (right side of the picture) which illustrates the enlarged and amoeboid morphological features of activated microglia cell bodies (Fig. 9 a, b).

In addition, the number of microglial cells and astrocytes increases in spinal dorsal horn ipsilaterally to a peripheral nerve injury (Fig. 9 a, b) while, approaching the ventral horn, both sides show the typical resting microglia morphology with no longer differences between ipsi- and contralateral side (Fig. 9, c, d, e).

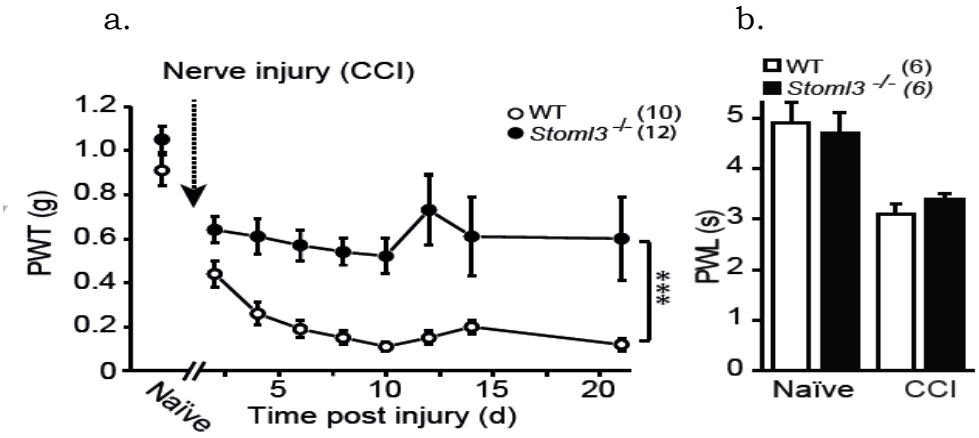

Figure 8. (a) Baseline withdrawal thresholds did not differ in wild type and *Stoml3*$^{-/-}$ mice before the surgery (naïve mice). After being subjected to CCI, wild type mice developed within a few days a full-blown allodynia with mechanical thresholds for paw withdrawal decreasing from 1.2 g to 0.04 g until the end of the measurements. In contrast, STOML3 null mice did not show any mechanical hyperalgesia until the third day of lesion, and mechanical threshold decreased to 0.6 g until the end of the observation period. **(b)** Thermal hyperalgesia symptoms were developed with the withdrawal latency dropping down from 5 seconds to 3 seconds. Thermal withdrawal thresholds did no differ between control and STOML3 null mice.

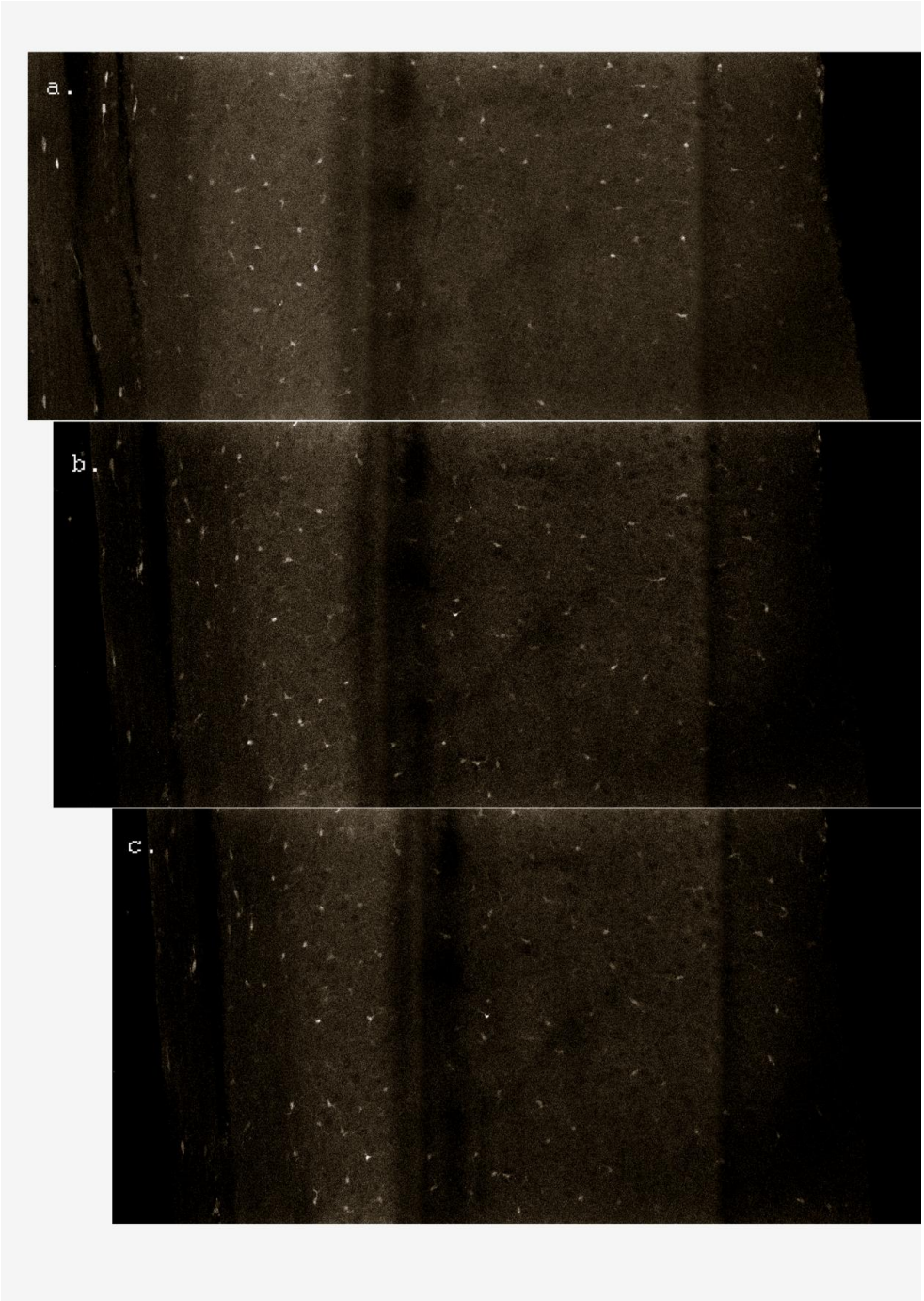

Figure 9. Confocal images of lumbar Spinal Cord from naïve McGreen mice show an equal microglia distribution between spinal cord antimeres from dorsal to ventral horn (a, b, c). Magnification: 10X.

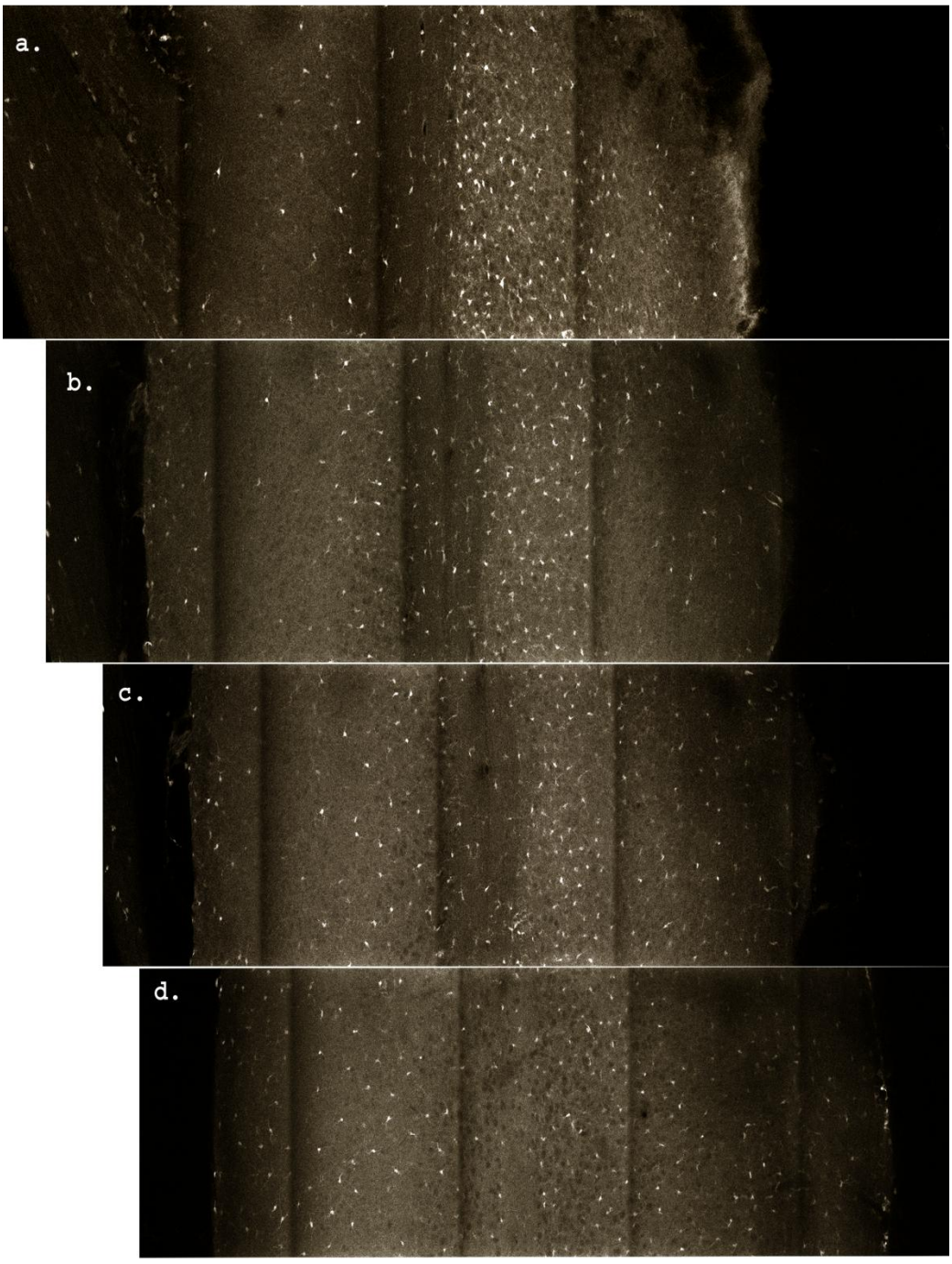

Figure 10. **(a,b)** Nerve injury induces marked microglial reaction in the ipsilateral lumbar spinal cord. The contralateral side (left) shows the typical resting microglial morphology; the ipsilateral side (right) illustrates the enlarged and amoeboid morphological features of activated microglia cell bodies. Approaching the ventral horn, microglia shows the typical resting morphology and no longer differs between the ipsi- and contralateral sides **(c, d, e).** Magnification: 5X.

3.4 Stoml3 gene expression in CCI mice

Wild type mice were subjected to unilateral CCI; after assessing the development of mechanical allodynia symptoms by using Von Frey hairs as described before, L4-L5 DRGs were dissected out and processed in order to investigate Stoml3 mRNA copy number in injured and uninjured side. In parallel, lumbar DRGs from naïve mice were also processed in order to obtain endogenous Stoml3 mRNA copy number.
Consistently with the histological data, qPCR revealed a quite low basal expression of Stoml3 transcript; copy number did not differ between left and right lumbar DRGs of naive mice. However, Stoml3 mRNA levels in L4-L6 DRGs that project axons to the ligation site was doubled compared to the control (mRNA copy no. 75.57±1.54 compared to 34.9±0.72, $p<0.05$; Mann-Whitney U test). By contrast, contralateral to the injury side no changes in Stoml3 transcript levels were observed (Fig. 10 f).

Analysis from *Stoml3^{lacZ}* mice revealed that STOML3 endogenous expression is restricted to large- and medium-sized cells; in addition, qPCR revealed a remarkable up-regulation of Stoml3 transcript in lumbar DRGs that project to the injured side. By means of X-gal staining, as described before, I next investigated STOML3 expression pattern under neuropathic conditions in *Stoml3$^{lacZ/+}$* heterozygous mice, in which only one allele is replaced by the *β-galactosidase* cassette.
Since genomic manipulation can alter the mice phenotype, in order to verify whether *Stoml3$^{lacZ/+}$* heterozygous mice displayed a normal mechanical sensitivity, mice were subjected to CCI in order to induce neuropathic pain; Von Frey up-down method was used to assess the development of neuropathic symptoms as described before. Mice displayed no differences in mechanical sensitivity in both paws before the lesion, while the development of mechanical hyperalgesia identical to that occurring in wild type mice was measured in the post-injury early stage until the end of the assessment (data not shown).
Lumbar DRGs from ipsi- and contralateral side to the injury were then dissected out and processed for X-gal staining. In heterozygous mice the staining appeared weaker

than that detected in *Stoml3*^{lacZ}. However, morphometric analysis of histological slices obtained from lumbar DRGs located in the lesion side displayed a number of lacZ-positive neurons more than doubled and with a more robust staining compared to the contralateral ones (105 stained cells in ipsilateral compared to 55 in contralateral DRGs; $p<0.001$, Chi-squared test). Again, cells fell predominantly in the large- to medium-size range, corroborating qPCR data on Stoml3 mRNA and the above reported results on the STOML3 endogenous expression pattern.

Surprisingly, only DRG slices from the unilateral lesion side revealed a positive staining localized to cellular elements in the epineurium, possibly of immune nature, suggesting that under neuropathic conditions STOML3 might go through a phenotypic plasticity which increases the pain hypersensitivity.

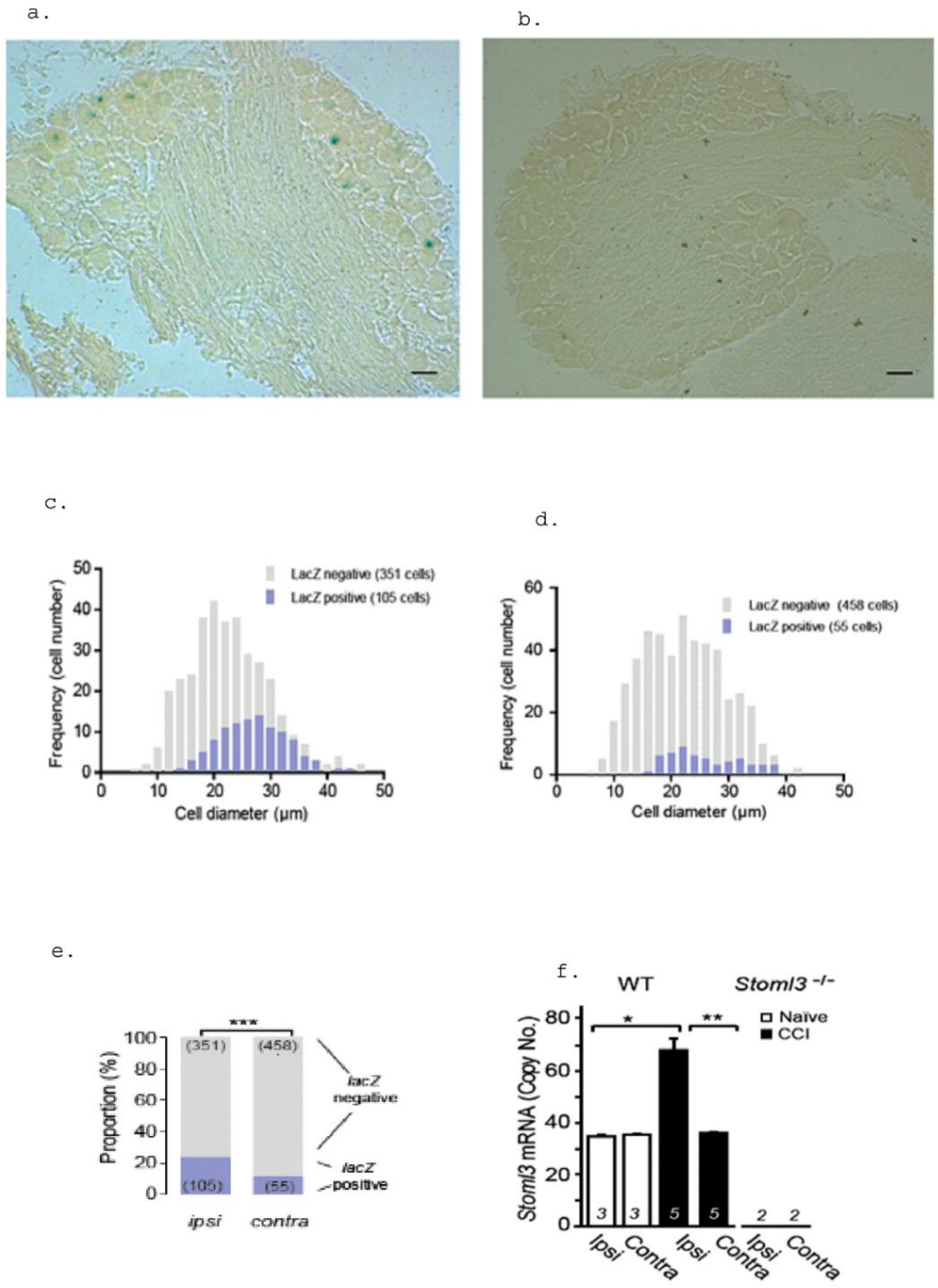

Figure 11. Immunostaining from *Stoml3*$^{+/LacZ}$ mice that had received the chronic constriction injury (CCI) shows an increase of stained cells in the ipsilateral DRGs **(a)** compared to the contralateral **(b).** LacZ-positive neurons fell predominantly in large cells in the ipsi-**(c)** and contralateral **(d)** DRGs. The number of LacZ positive neurons is significantly increased after CCI (***p<0.001; Chi-squared test; data are displayed as percentage neurons). **(f)** Stoml3 copy number derived from L4-6 (two mice per preparation) determined using real-time PCR shows an ipsilateral up-regulation of Stoml3 mRNA; the two last bars represent data from *Stoml3*$^{-/-}$ mice (**p<0.01, *p<0.05; Mann-Whitney U test; error bars indicate s.e.m.).

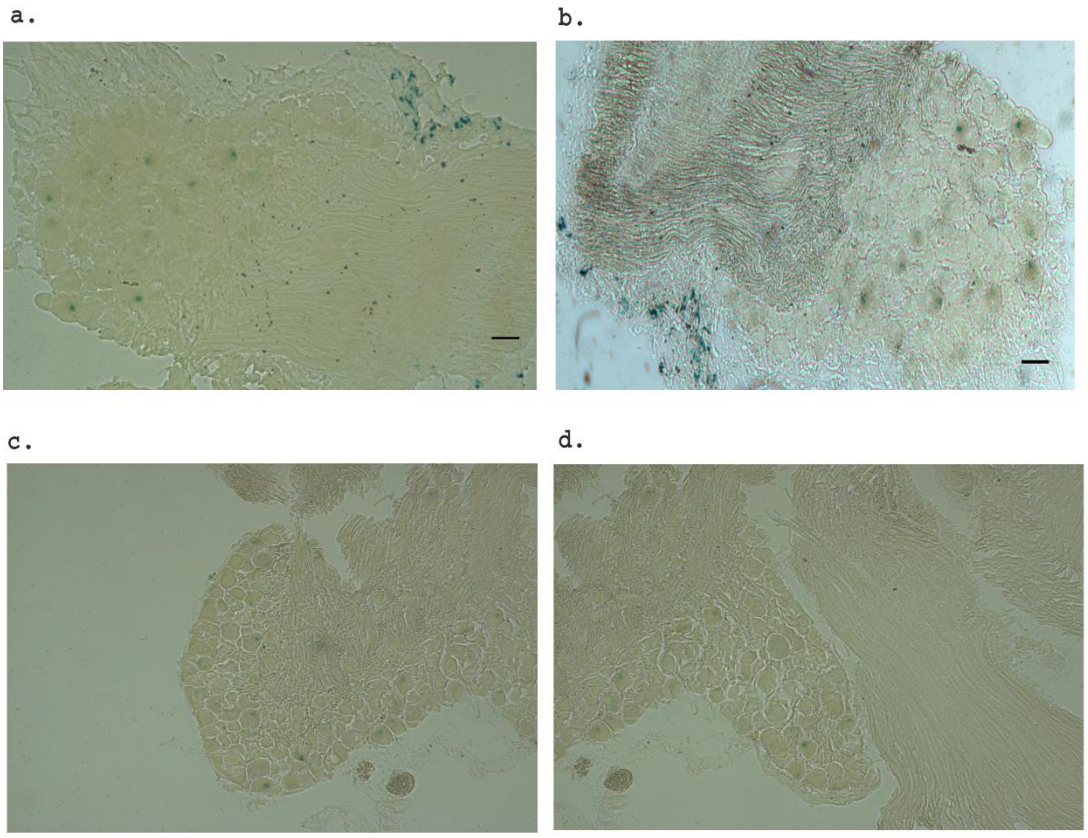

Figure 12. Lumbar DRGs show a de novo staining after CCI. X-gal staining of lumbar DRGs from *Stoml3*$^{+/LacZ}$ mice that received the nerve injury revealed positive cells in the epineurium of ganglia ipsilateral to the injury **(a, b)** which is not detectable in contralateral ganglia from the same mice **(c, d).** Bar-40 µm.

3.5 Effect of peripheral STOML3 blockade on tactile allodynia in neuropathic mice

Many cutaneous mechanoreceptors in *Stoml3*$^{-/-}$ mice innervate the skin but cannot be activated by mechanical stimulation (Moshourab et al., 2013; Wetzel et al., 2007); in addition, STOML3 null mice are largely protected from tactile allodynia symptoms, but not from the thermal hyperalgesia. These observations led to hypothesize that modulation of mechanotransduction could somehow control the severity of neuropathic pain symptoms through STOML3 modulation.

It has been recently demonstrated that the modulation of mechanotransduction by STOML3 depends on his capability to oligomerize (Brand et al., 2012); in order to identify a compound that would be able to disrupt or even enhance STOML3 function, a huge screening of molecules by using *Bimolecular Fluorescence Complementation assay* (BiFC) was made. With this assay the site of protein–protein interaction can be monitored as a fluorescence signal in cells when two fragments of a fluorescent protein fused to interacting proteins come together (Hu and Kerppola, 2003).

In particular, N- and C- terminal halves of YFP molecule are tagged to the intracellular termini of STOML3, that thus functions as prey and bait protein; when the two halves of YFP, located at the STOML3 C-terminus, come within 5 nm from each other, a fluorescent signal that increases linearly over time is producted. Mutations in one STOML3 pair that disrupt dimerization or higher order interactions that take place via stomatin-domain specifically reduce the rate of signal development.

After a preliminary screen of about 35000 small molecules obtained from the central compound collection at the FMP screening unit (www.chembionet.info), two inhibitors of STOML3 self-association, called Oligomerization Blocker 1 and 2 (OB-1 and OB-2) and two enhancers of STOML3 self-association called Oligomerization Enhancer 1 and 2 (OE 1 and OE-2) were found. By blocking STOML3 oligomerization it is possible to silence tactile afferents completely and specifically, so that many but not all nociceptive sensory neurons have unchanged sensitivity (data not shown).

OB-1 reverses tactile allodynia in CCI mice. Local subcutaneous injections of the OB-1 compound (250-500 pMol per paw) into the hairy skin of the mouse lateral foot innervated by saphenous nerve were done; application of OB-1 did not change withdrawal thresholds in naïve mice, as well as no difference was found between uninjured control and *stoml3*$^{-/-}$ mice; in addiction, no change in withdrawal latency for radiant heat stimuli was measured and OB-1 application to *Stoml3*$^{-/-}$ mice subjected to unilateral CCI did not reveal any difference between the ipsi- and contralateral paw (Fig. 12 a, b, c).

Mice were thus subjected to unilateral CCI, and mechanical symptoms development was assessed by Von Frey adapted up-and-down method as described before. Following neurophatic symptoms fully development, a blinded interplantar injection of OB-1 to the paws of wild type mice with established neuropathic pain was done; it was then possible to observe a complete reversal of the tactile allodynia (0.075±0.02 g CCI mice vs 1.13±0.5 OB1 treated, Fig. 12 d).

The effect is maximal after 3 hours of injection consistent with the idea that OB-1 prevents oligomerization of STOML3; the effects of OB-1 on tactile allodynia wore off slowly over the next 12 hours so that the effect was absent after 24 h (data not shown); The reversal of tactile allodynia was indistinguishable from that found with systemic gabapentin treatment (Fig. 12 e), a standard centrally acting drug in clinical use for the treatment of neuropathic pain (Dworkin et al., 2010). Application of a series of OB-1 concentration on the neuropathic paw allowed determining a half-maximal effective dose (ED_{50}) of 4.42 μM (or approximately 20 pmol per paw) (Fig. 12, f).

OB-1 does not affect *Stoml3* gene expression. OB-1 is able to prevent STOML3 dimerization and higher order of oligomerization, affecting the native mechanosensitivity currents similar to the results obtained from *Stoml3*$^{-/-}$ mice; intraplantar local injection of OB-1 has been shown to revert mechanical hyperalgesia symptoms in CCI mice, in which Stoml3 mRNA is significantly up-regulated. Thus, I next asked whether the effect of OB-1 and OE-1 could lead to changes on Stoml3

mRNA transcript. We thus exposed acutely isolated sensory neurons to 20 μM of each OB-1 and OE-1 for 3 hours in order to measure stoml3 mRNA copy number. qPCR revealed that OB-1 and OE-1 treatment do not lead to any change in the level of stoml3 mRNA transcript (Fig. 12 g). Cultured N2A cells were treated as well for 3 hours with 20 μM of OB-1 and OE-1. Again, qPCR did not display any change in mRNA copy number, suggesting that these molecules exert their effect without regulating Stoml3 gene expression.

Inflammatory pain is not dependent on STOML3. Systemic dosing with Nerve Growth Factor provokes inflammatory pain. In this model mechanical and thermal hyperalgesia are prominent features, and they are largely dependent on an increased NGF level (Lewin et al., 2014). Systemic injection of NGF (1 mg/kg) in naïve and *Stoml3*$^{-/-}$ mice provokes long lasting mechanical and thermal hyperalgesia in both mice strains without any remarkable difference; in addition, these symptoms are not reversed by local application of OB-1 (Fig. 13 a), suggesting that heat hyperalgesia is not dependent on STOML3and thus is not influenced by OB-1 effect.

STOML3 is the major target in OB-1 mediate symptom relief. Neuropathic pain can be induced by means of several models. CCI model cause a direct damage to the axons that innervate the skin of the plantar hindpaw (Basbaum et al., 1991). However, other models that cause hyperalgesia to the skin in the same part of the leg do not involve direct injury to the sensory afferents. Spare nerve injury (SNI) induces hypersensitivity of the plantar hind-paw by cutting nerves adjacent to the tibial nerve that supplies both efferent and afferent innervation to the plantar foot (Decosterd et al., 2000; Shields et al., 2003).

Wild type mice were subjected to SNI, and then Von Frey up and down test was used to monitorate the development of allodynia as described before. Mice showed a long lasting mechanical hypersensitivity of a similar magnitude to that observed in CCI with the average of withdrawal threshold ranging from 1 g before the surgery to 0.004 g few days after the surgery until the end of the measurements (Fig. 14, a).

A local dose of OB-1 was then injected as described before; surprisingly, application of OB-1 to the plantar skin did not produce reversal of mechanical hypersensitivity (Fig. 14, b)

We next dissected out lumbar DRGs from SNI mice in order to investigate Stoml3 mRNA level by quantitative real-time PCR. Interestingly, no changes of mRNA transcripts levels between the injured and uninjured side was found in this model (Fig. 14, c), suggesting that the up-regulation of STOML3 in CCI model is pathophysiologically relevant for the development of touch hypersensitivity in this model , and thus that STOML3 as the major target in OB-1 mediate symptom relief.

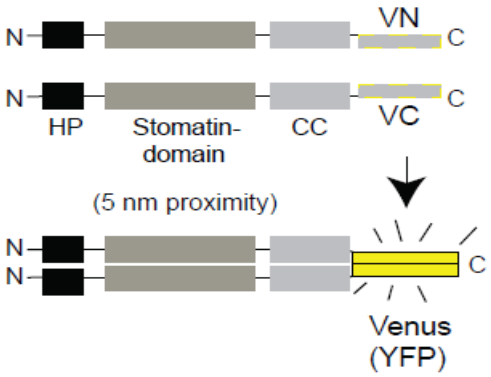

Figure 13. Self-association of stomatin-domain proteins can be monitored using BiFC whereby N-and C-terminal halves of YFP molecule are tagged to the prey and bait protein STOML3. Wild type STOML3 was used as both the bait and the prey.

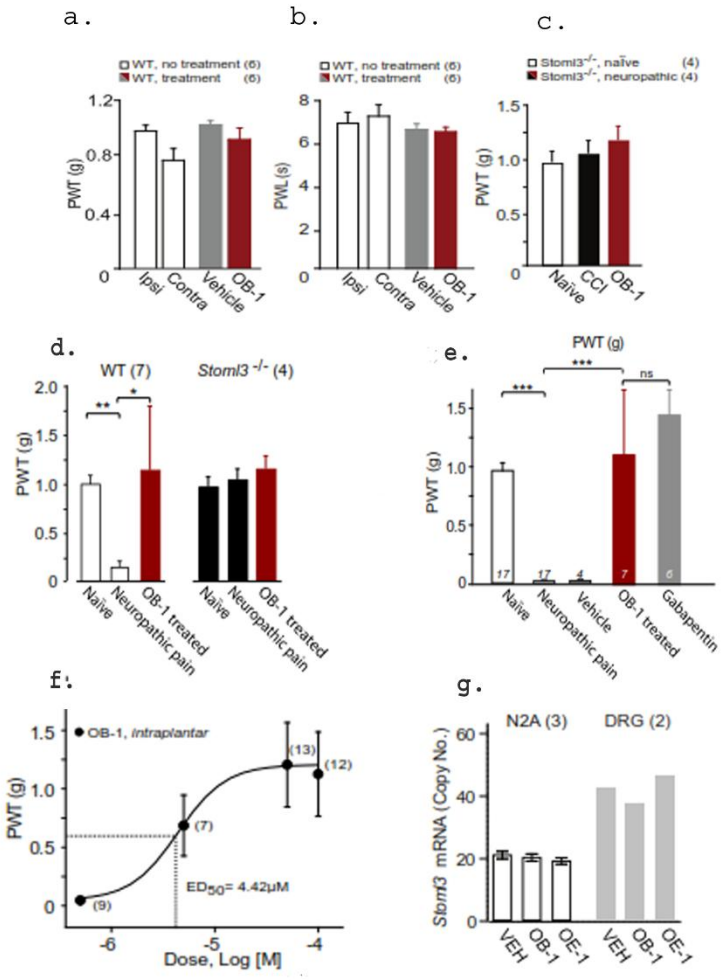

Figure 14. (a) Paw withdrawal thresholds (PWT) show that naïve mice do not respond to local OB-1 interplantar treatment. **(b)** Paw withdrawal latencies (PWT) to a radiant heat beam applied to the hind paw show that naïve wild type mice do not respond to OB-1 treatment. **(c)** PWTs of STOML3 null mice do not change after localOB-1 treatment. **(d)** PWTs show that *Stoml3*$^{-/-}$ mice develop significantly less touch-evoked pain symptoms compared to wild type animals (***p<0.001, two-way ANOVA). **(e)** After interplantar application of OB-1 to the paw of mice with established neuropathic pain, a complete reversal of tactile-evoked pain can be observed (OB-1 treated p<0.001; Mann Whitney U-test); OB-1 relieve of touch-evoked pain is indistinguishable from gabapentin treated mice **(f)** OB-1 has an half-maximal effective dose (ED_{50}) of 4.42 µM (approximately 20 pmol per paw). **(g)** N2A cells and acutely isolated DRGs were treated with either vehicle, OB-1 orOE-1 (20 µM) for 3 hour before mRNA isolation, reverse transcription and qRT-PCR; no difference in Stoml3 transcript was detected.

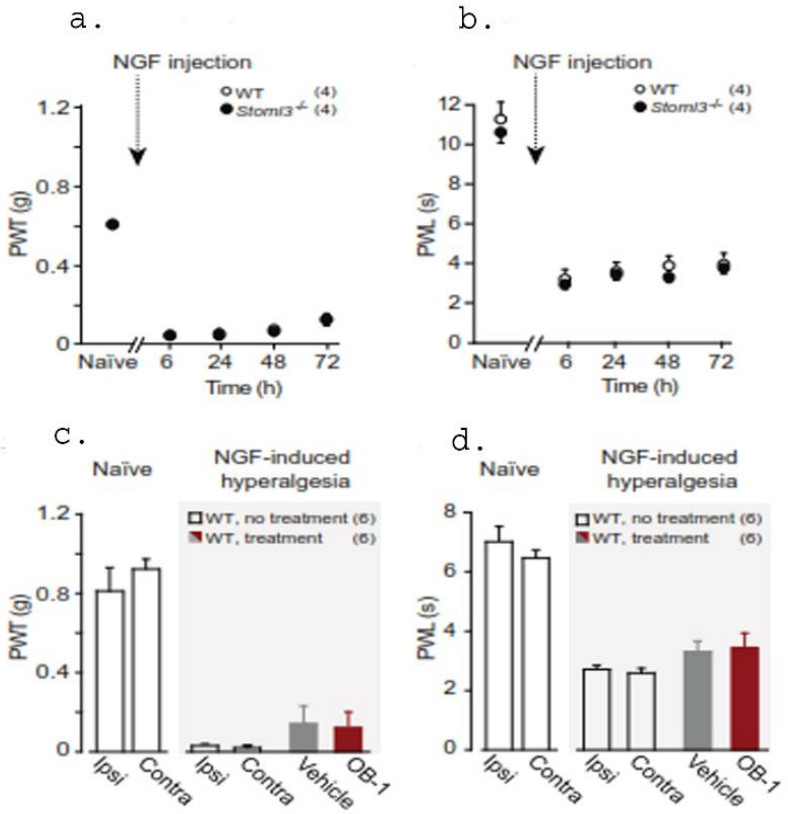

Figure 15. (a, b) PWTs and PWLs before and after NGF-induced hyperalgesia indicate no changes between genotypes. **(c, d)** OB-1 do not alleviate NGF-induced mechanical and thermal hyperalgesia. Numbers indicate mice treated; data are displayed as mean PWL/PWL ± s.e.m.

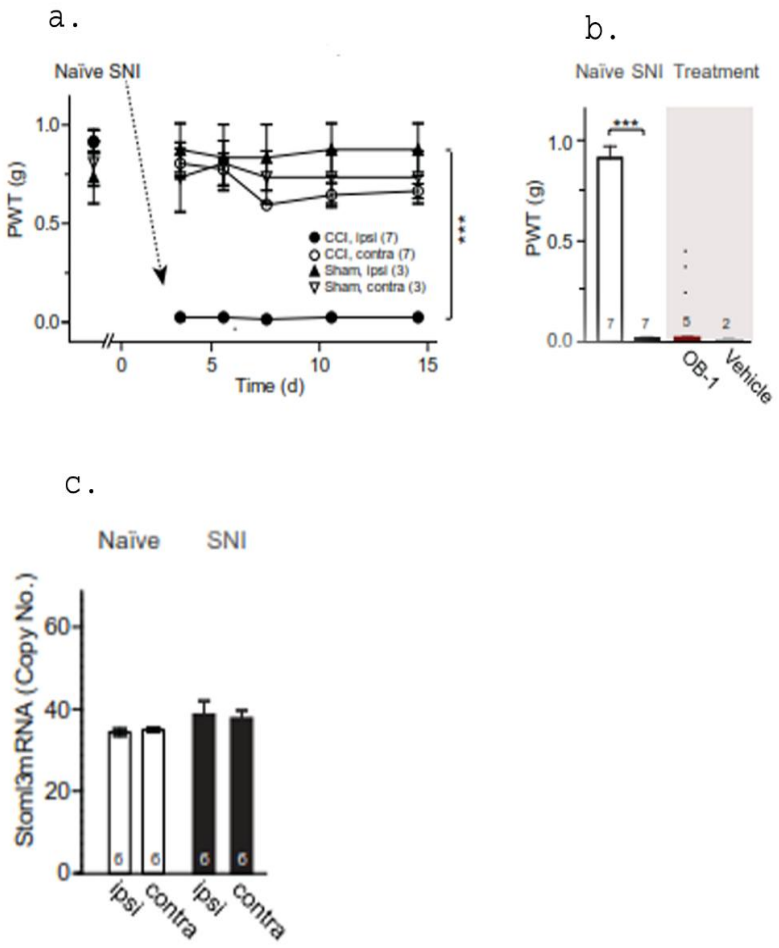

Figure 16. (a) Development of tactile-evoked pain using the spare nerve injury (SNI) model. Wild type mice develop a prolonged tactile-evoked pain ipsilateral to the injury (***p<0.001; Two way ANOVA; error bars indicate s.e.m.). **(b)** PTWs are measured showing no alleviation of tactile-evoked pain after local OB-1 treatment. **(c)** Stoml3 copy number from lumbar DRGs determined using real-time PCR showed no up-regulation of Stoml3 mRNA after SNI.

4. Discussion

The DRG primary sensory neurons transduce mechanical signals at their nerve endings via mechanically-gated ion channels, the activation of which depolarizes nerve endings to initiate spikes (Drew, Wood, & Cesare, 2002; Hu & Lewin, 2006; Lechner & Lewin, 2013; McCarter, Reichling, & Levine, 1999), detecting the sense of touch and pain.

Mammals touch sensation still remains poorly understood at the molecular level, even though recent findings of novel families of proteins acting as mechanosensing molecules has undoubtedly accelerated our understanding of mechanotransduction mechanisms in mammalian somatosensation. Recent data indicate that Piezo2 is the critical transducer of mechanical stimuli in sensory neurons, and its sensitivity can be modulated by STOML3 by nanometer-scale stimuli (Poole et al., 2014; Ranade et al., 2014; Schrenk-Siemens et al., 2015; Wetzel et al., 2007).

STOML3 has been demonstrated to be necessary for the function of at least 35% of the mechanoreceptors; in addition STOML3 null mice are also largely protected from touch-evoked pain under neuropathic conditions (Wetzel et al., 2007).

Neuropathic pain is a debilitating condition whose key feature is represented by the so-called touch-evoked pain, initiated upon activation of low threshold mechanoreceptors (Costigan et al., 2009; Lewin & Moshourab, 2004; von Hehn et al., 2012; Tal & Bennet, 1994). The remarkable protection from touch-evocked pain in STOML3 null mice lead to hypothesize a role for STOML3 in neuropathic pain; in that case, enhancing or inhibiting touch sensitivity with small molecules would be desirable for treating a variety of sensory disorders. Inhibition of touch receptor function could be then used to treat the extreme pain experienced by neuropathic pain patients when subjected to the slightest brush of a feather (Costigan et al., 2009; von Hehn et al., 2012).

The data presented on this thesis revealed that STOML3 is a key contributor in a murine model of neuropathic pain and a promising target in neuropathic pain

treatment through the modulation of mechanoreceptor function at the level of transduction with small molecule inhibitors of STOML3 oligomerization.

STOML3 *in-vivo* expression pattern.

Spinal cord. Consistent with previous qPCR data, immunohistochemical analysis carried out in the spinal cord showed a staining restricted to cells surrounding the central canal and few other cells in the gray matter. The central canal is a cerebrospinal fluid (CSF) -filled cavity that runs through the spinal cord is continuous anteriorly with the ventricular system of the brain and enlarges at the region of the obex to become the 4th ventricle. It represents the remainder of the neural canal in adults, and is lined with ependyma, a thin epithelium-like membrane composed by ependymal cells, a neuroglia cell-type with several recognized roles among which the CSF production and circulation through the ventricular cavities. It has been reported that in the spinal cord, central canal ependymal cells possess latent neural stem cell properties and that injury induces proliferation of ependymal cells and migration of ependyma-derived progeny towards the site of injury (Meletis et al., 2008; Hamilton et al., 2009; Mothe & Tator, 2005; Marichal et al., 2009). Considering that STOML3 shows a preferential neuronal expression, future phenotypical characterization of the STOML3-βgal positive ependymal-like cells with such markers like doublecortin (DCX) and poly-sialylated neuronal cell adhesion molecule (PSA-NCAM), typical of migrating neuroblasts, should be done in order to verify their nature.

Lumbar DRGs. qPCR data revealed a quite low expression of mRNA copy number in L4-L6 DRGs; further histological analysis allowed me to show that *Stoml3* expression is restricted to large- and medium-sized neurons, which fell in the range of Aβ- and Aδ-fibers, respectively.

Almost all large diameter sensory neurons isolated from wild type mice possess a fast and sensitive mechanically gated current (Hu, Chiang, Koch, & Lewin, 2010; Hu & Lewin, 2006; Lechner et al., 2009). Mechanosensitive currents require the presence of STOML-3, as they were absent in large diameter neurons isolated from *Stoml3*$^{-/-}$ mice

and could be rescued after reintroduction of a cDNA encoding wild type STOML-3 (Wetzel et al., 2007). Thus, it can be assumed that the reported lack of mechanosensitivity is due to a restricted expression of STOML3 to a distinct subpopulation of mechanosensitive sensory neurons.

Stoml3 decreases with ageing. An age-related decline in the main sensory modalities is well reported; therefore, a loss of mechanosensitivity with advancing age would be expected. However, studying and interpreting the effect of ageing on touch is still matter of studies. Some studies have pointed out a change in peripheral components of touch perception with advancing age, highlighting that ageing influences several morphological and functional features of the peripheral nervous system. I thus asked whether a decrease of Stoml3 gene expression could be related to a loss of mechanosensitivity. Quantitative real-time PCR revealed a significant down-regulation of Stoml3 mRNA copy number in 12 weeks old mice compared to 42 weeks old mice, suggesting that a loss of the normal mechanosensitivity with ageing could be also related to decreasing of Stoml3 mRNA expression in sensory neurons. Electrophysiological properties of mechanosensitive currents in old mice are by now under investigation.

Stoml3 gene expression in CCI mice

STOML3 null mice are largely protected from touch-evoked pain after being subjected to a unilateral chronic constriction injury (Wetzel et al., 2007). Baseline paw withdrawal thresholds in wild type and *Stoml3*$^{-/-}$ mice did not differ, as measured with von Frey adapted *up-down* method. However, after induction of a unilateral CCI, paw withdrawal thresholds dropped profoundly in wild type mice but were only moderately reduced in *Stoml3*$^{-/-}$ mice.

The remarkable protection from touch-evoked pain in animals lacking STOML3 led to hypothesize that the nerve injury may itself lead to a change in the levels of Stoml3

mRNA expression in the DRG. Quantitative PCR measured a doubling in Stoml3 mRNA expression levels in the lumbar DRGs that project axons to the ligation site compared to control, while no change was found on the side contralateral to the injury. In addition, by using *Stoml3*$^{+/lacZ}$ knock in mice, I have also revealed a doubling in the number of lacZ positive neurons in the L6-L4 ipsilateral ganglia after a unilateral CCI, with stained cells that fell predominantly in the large to medium sized-range.
These data are consistent with the idea that chronic nerve constriction leads to an increase in the number of large and medium sized sensory neurons and that up-regulation of STOML3 could in turn exacerbate touch-evoked pain by enhancing the sensitivity of mechanotransduction in sensory afferents within the injured nerve.

Surprisingly, DRG epineurium displayed positive staining localized to cellular elements only restricted to lumbar DRGs that project to the CCI side.
Incomplete nerve damage by a CCI of the sciatic nerve induces pain behavior and is accompanied by a profound local inflammatory response which includes the infiltration of *immune cells* (Stoll and Muller, 1999; Sommer et al., 2001). Adult neuropathic pain is characterized by microglia activation, T-cells infiltration and the release of pro-inflammatory immune mediators in the dorsal horn, critical for sensibilization and pain-like hypersensitivity (Taves et al., 2013; Tsuda et al., 2013). Macrophages, neutrophils, CD4+ T-cells and immune-like glial cells (such as microglia) are known to respond to nerve injury by alterating intercellular signalling and by migrating to areas of inflammation within the peripheral and central nervous system (Ren et al., 2010).
It has been recently demonstrated that *degenerated peripheral nerves* are also infiltrated by T-cells (Moalem et al., 1999; Moalem et al., 2004); cytokine-mediate signalling and CD4+ T-cells have been shown to have a relevant contribution in the development of neuropathic pain (Sommer et al., 2004; Molaem et al., 2004). T-cells are the principal source of IL-17, have immune modulating properties and coordinates local tissue inflammation via the release of other pro-inflammatory cytokines and chemokines (Kolls & Linden 2004). Moreover, congenitally athymic nude rats, which lack mature T-cells, developed reduced mechanical allodynia and thermal hyperalgesia (Molaem et al., 2004).

It might be possible that *de novo* expression of STOML3 in T- cells, which may occur in neuropathic conditions, can also contribute at the mechano-hypersensitivity; additional analysis of co-localization with specific markers of immunological cells such as IL 17 has to be done in order to investigate the nature of cells that seem to acquire *de novo* the ability to express STOML3 only under neuropathic conditions.

Effect of STOML3 peripheral blockade in neuropathic pain

The modulation of mechanotransduction by STOML3 is dependent on its ability to oligomerize (Brand et al., 2012; Poole et al., 2014). This key fact prompted to design a small molecule strategy to modulate STOML3 activity and thereby mechanoreceptor sensitivity. Molecules that decrease STOML3 self-association block the ability of STOML3 to modulate Piezo channels and small molecules that enhance STOML3 self-association can sensitize Piezo channels to molecular scale movements. The discovery of mechanotransduction modulating drugs opens the possibility that optimized lead molecules that are active peripherally can be rapidly developed to treat this condition.

By blocking STOML3 oligomerization it can be possible to silence tactile afferents completely and specifically, so that many but not all nociceptive sensory neurons have unchanged sensitivity (data not shown). The results presented in this thesis revealed that OB-1 treatment on CCI mice reverses well-established touch-evoked neuropathic symptoms. In addition, quantitative Stoml3 mRNA analysis revealed no changes of Stoml3 gene expression in lumbar DRGs and N2A cells after OB-1 treatment for 3 hours, consistent with the hypothesis that the compound do not affect gene expression but it only silences tactile afferents blocking STOML3 oligomerization at the protein level. The effect of OB-1 is local and reversible after 24 hours from the treatment, leading to control touch sensitivity in vivo with both temporal and spatial precision without affecting the axon excitability *in vivo* (data not shown). In addition, the observation that OB-1 has no effect in changing *Stoml3*$^{-/-}$ paw withdrawal thresholds led to assume that the compound effects do not take place via

other Stomatin domains, but that STOML3 is the main effector of OB-1 mediated symptom relief.

Chronic constriction injury (CCI) represent a model of well established neuropathic symptoms which can be well related to the human condition; however, it does not enable injured and not-injured axons to be identified. Furthermore, it has been demonstrated a near complete loss of large myelinated fibers distal to the ligature in rat (Basbaum, 1991).

By using one variant of the spared nerve injury model (SNI) in mice, new experiments were carried out, whose results were surprising but provide new insight into the role of STOML3 in driving neuropathic pain. Von Frey thresholds on the side ipsilateral to the injury dropped to levels comparable to those observed in CCI model; however, OB-1 compound did not reverse the mechanical hypersensitivity.

The main difference between these two models of induced peripheral neuropathies is that many of the axons that innervate the sensitized area of the foot in the CCI model are indeed directly damaged; in contrast, the afferents innervating the sensitized area in SNI model are not damaged. In addition, minor changes in mechanoreceptors function have been shown to occur in the spinal nerve ligation model (Na et al., 1993).

I revealed that Stoml3 mRNA is selectively up-regulated in DRG neurons subjected to a neuropathic nerve injury; however, I did not observe any changes in Stoml3 expression in sensory neurons subjected to axotomy *per se*.

These data suggest that physiological changes in injured afferents may be dependent on STOML3 regulation and significantly contribute to the severity of neuropathic pain symptoms; thus, the analgesic effect of OB-1 seems to be associated with a relevant up-regulation of STOML3 in CCI damaged sensory afferents.

In conclusion, the data presented in this thesis show that STOML3 is an important contributor and a promising pharmacological target in a mouse model of chronic neuropathic pain, and that by targeting STOML3 oligomerization with small molecules it can be possible tuning mechanotransduction in either direction, to inhibit or enhance sensitivity, leading the possibility of treating the mechanical hyperalgesia symptoms of several forms of neurological disorders where touch sensation is disturbed.

References

Aldskogius, Ê. K. a N., & Kozlova, E. N. (1998). Central Neuron ± Glial and Glial ± Glial Interactions Following Axon Injury, *55*(97).

Baker, M. D., & Wood, J. N. (2001). Involvement of Na+ channels in pain pathways. *Trends in Pharmacological Sciences*, *22*(1), 27–31.

Basbaum A. I., Levine J. D. (1991) The contribution of the nervous system to inflammation and inflammatory disease. *Can J Physiol Pharmacol.* 69(5), 647-51.

Beggs, S., Trang, T., Salter, W. M. (2012) $P2X4R^{+}$ microglia drive neuropathic pain. *Nature Neuroscience,* 15, 1068–1073.

Bennett, G. J., & Xie, Y. K. (1988). A peripheral mononeuropathy in rat that produces disorders of pain sensation like those seen in man. *Pain*, *33*, 87–107.

Brand, J., Smith, E. S. J., Schwefel, D., Lapatsina, L., Poole, K., Omerbašić, D., … Daumke, O. (2012). A stomatin dimer modulates the activity of acid-sensing ion channels. *The EMBO Journal*, *31*(17), 3635–3646.

Chalfie, M., & Sulston J. Developmental genetics of the mechanosensory neurons of Caenorhabditis Elegans (1981) *Developmental Biology*., 82, 358-370.

Chaplan, S. R., Bach, F. W., Pogrel, J. W., Chung, J. M., Yaksh, T. L. Quantitative assessment of tactile allodynia in the rat paw (1994) *Journal of Neuroscience Methods*, 53(1), 55-63.

Chen Y., Devor M. (1998) Ectopic mechanosensitivity in injured sensory axons arises from the site of spontaneous electrogenesis. *European Journal of Pain, 2,* 165–178

Chung K., Wallace, J., Kim, S., … Gradinaru, V., & Deisseroth K. (2013) Structural and molecular interrogation of intact biological systems. *Nature*, 497, 332-337

Coste, B., Mathur, J., Schmidt, M., Earley, T. J., Ranade, S., Petrus, M. J., … Patapoutian, A. (2010). Piezo1 and Piezo2 are essential components of distinct mechanically-activated cation channels Bertrand. *Science*, 330(6000), 55–60.

Costigan, M., Scholz, J., & Woolf, C. J. (2009). Neuropathic pain: a maladaptive response of the nervous system to damage. *Annual Review of Neuroscience 32*, 1–32.

Stoll G., Jander S. (1999). The role of microglia and macrophages in the pathophysiology of the CNS. *Prog Neurobiol* 58, 233–247.

Decosterd I, Woolf CJ (2000). Spared nerve injury: an animal model of persistent peripheral neuropathic pain. *Pain* 87, 149-158.

Devor, M., Jänig, W., & Michaelis, M. (1994). Modulation of activity in dorsal root ganglion neurons by sympathetic activation in nerve-injured rats. *Journal of Neurophysiology*, 71(1), 38–47.

Drew, L. J., Wood, J. N., & Cesare, P. (2002). Distinct mechanosensitive properties of capsaicin-sensitive and -insensitive sensory neurons. *The Journal of Neuroscience: The Official Journal of the Society for Neuroscience*, 22(12), RC228.

Goldstein B. J., Kulaga H. M., Reed R. R. (2003) Cloning and characterization of SPL3: a novel member of the stomatin family expressed in olfactory receptor neurons. *Journal of the Association for research in Otolaryngology* , 4(1), 74-82

Goodman, M. B., Ernstrom, G. G., Chelur, D. S., O'Hagan, R., Yao, C. A., & Chalfie, M. (2002). MEC-2 regulates C. elegans DEG/ENaC channels needed for mechanosensation. *Nature*, 415(6875), 1039–1042.

Green, J. B., & Young, J. P. W. (2008). Slipins: ancient origin, duplication and diversification of the stomatin protein family. *BMC Evolutionary Biology*, *8*, 44.

Gwak, Y. S., Crown, E. D., Unabia., G. C., Hulsebosch, C. E. (2008). Propentofylline attenuates allodynia, glial activation and modulates GABAergic tone after spinal cord injury in the rat. *Pain*, 138(2) 410-422

Hamilton, L. K., Truong, M. K. V, Bednarczyk, M. R., Aumont, a., & Fernandes, K. J. L. (2009). Cellular organization of the central canal ependymal zone, a niche of latent neural stem cells in the adult mammalian spinal cord. *Neuroscience*, *164*(3), 1044–1056.

Hu, J., Chiang, L.-Y., Koch, M., & Lewin, G. R. (2010). Evidence for a protein tether involved in somatic touch. *The EMBO Journal*, 29, 855–867.

Hu, J., & Lewin, G. R. (2006). Mechanosensitive currents in the neurites of cultured mouse sensory neurones. *The Journal of Physiology*, 577, 815–828.

Hu C. D., Kerppola T. K. (2003) Simultaneous visualization of multiple protein interactions in living cells using multicolor fluorescence complementation analysis. *Nature Biotechnology.,* 21, 539-545.

Kim, K. J., Yoon, Y. W., & Chung, J. M. (1997). Comparison of three rodent neuropathic pain models. *Experimental Brain Research*, 113, 200–206.

Kobayakawa, K., Hayashi, R., Morita, K., Miyamichi, K., Oka, Y., Tsuboi, A., & Sakano, H. (2002). Stomatin-related olfactory protein, SRO, specifically expressed in the

murine olfactory sensory neurons. *The Journal of Neuroscience : The Official Journal of the Society for Neuroscience*, 22(14), 5931–5937.

Kolls, J. K. & Linden, A. (2004). Interleukin-17 family members and inflammation. *Immunity*, 21(4), 467-476.

Lapatsina, L., Brand, J., Poole, K., Daumke, O., & Lewin, G. R. (2012). Stomatin-domain proteins. *European Journal of Cell Biology*, 91(4), 240–245.

Lawson, S. N. (1992). Morphological and biochemical cell types of sensory neurons. *Sensory Neurons: Diversity, development, and plasticity*. New York (USA): Oxford University Press. p. 27-52

Lechner, S. G., Frenzel, H., Wang, R., & Lewin, G. R. (2009). Developmental waves of mechanosensitivity acquisition in sensory neuron subtypes during embryonic development. *The EMBO Journal*, 28(10), 1479–1491.

Lechner, S. G., & Lewin, G. R. (2013). Hairy sensation. *Physiology (Bethesda, Md.)*, 28(3), 142–150.

Lewin, G. R., & Moshourab, R. (2004). Mechanosensation and pain. *Journal of Neurobiology*, 61(1), 30–44.

Marichal N., García G., Radmilovich M., Trujillo-Cenóz O. & Russo R. E. (2009) Enigmatic central canal contacting cells: immature neurons in "standby mode"? *Journal of Neuroscience* 29, 10010-10024

McLachlan E. M., Jänig W., Devor M., Michaelis M. (1993) Peripheral nerve injury triggers noradrenergic sprouting within dorsal root ganglia. *Nature* 363, 543–546.

McCarter, G. C., Reichling, D. B., & Levine, J. D. (1999). Mechanical transduction by rat dorsal root ganglion neurons in vitro. *Neuroscience Letters*, *273*(3), 179–182.

McCarthy, P. W., & Lawson, S. N. (1990). Cell type and conduction velocity of rat primary sensory neurons with calcitonin gene-related peptide-like immunoreactivity. *Neuroscience*, 34(3), 623–632.

Meletis K., Barnabé-Heider F., Carlén M., Evergren E., Tomilin N., Shupliakov O. & Frisén J. (2008) Spinal cord injury reveals multilineage differentiation of ependymal cells. *PLoS Biology* 6**,** e182

Miki, K., Fukuoka, T., Tokunaga, a, & Noguchi, K. (1998). Calcitonin gene-related peptide increase in the rat spinal dorsal horn and dorsal column nucleus following peripheral nerve injury: up-regulation in a subpopulation of primary afferent sensory neurons. *Neuroscience*, 82(4), 1243–1252.

Milligan, E. D., Zapata, V., Chacur, M., Schoeniger, D., Biedenkapp, J., O'Connor, K. a., … Watkins, L. R. (2004). Evidence that exogenous and endogenous fractalkine can induce spinal nociceptive facilitation in rats. *European Journal of Neuroscience*, 20, 2294–2302.

Moalem, G., Leibowitz-Amit, R., Yoles, E., Mor, F., Cohen, I., R. & Schwartz, M. (1999) Autoimmune T-cells protect neurons from secondary degeneration after central nervous system axotomy. *Nature Medicine*, 5, 49-55.

Moalem, G., Xu, K., Yu, L. (2004). T-lymphocyte play a role in neuropathic pain following peripheral nerve injury in rats. *Neuroscience*, 129, 767-777.

Moshourab, R. a, Wetzel, C., Martinez-Salgado, C., & Lewin, G. R. (2013). Stomatin-domain protein interactions with acid-sensing ion channels modulate nociceptor mechanosensitivity. *The Journal of Physiology*, 591(22), 5555–5574.

Mothe, A., & Tator, C. (2005). Proliferation, migration, and differentiation of endogenous ependymal region stem/progenitor cells following minimal spinal cord injury in the adult rat. *Neuroscience*, 131, 177–187.

Na, H. S., Leem, J. W., Chung, J. M. (1993) Abnormalities of mechanoreceptors in a rat model of neuropathic pain: possible involvement in mediating mechanical allodynia. *Journal of Neurophysiology*, 70, 522-528.

O'Hagan, R., Chalfie, M., & Goodman, M. B. (2005). The MEC-4 DEG/ENaC channel of Caenorhabditis elegans touch receptor neurons transduces mechanical signals. *Nature Neuroscience*, 8(1), 43–50.

Poole, K., Herget, R., Lapatsina, L., Ngo, H.-D., & Lewin, G. R. (2014). Tuning Piezo ion channels to detect molecular-scale movements relevant for fine touch. *Nature Communications*, 5, 3520.

Price, M. P., McIlwrath, S. L., Xie, J., Cheng, C., Qiao, J., Tarr, D. E., … Welsh, M. J. (2001). The DRASIC cation channel contributes to the detection of cutaneous touch and acid stimuli in mice. *Neuron*, 32(6), 1071–1083.

Ren, K., & Dubner, R. (2010) Interactions between the immune and nervous system in pain. *Nature medicine*, 16(11), 1267-1276.

Ranade, S. S., Woo, S.-H., Dubin, A. E., Moshourab, R. A., Wetzel, C., Petrus, M., … Patapoutian, A. (2014). Piezo2 is the major transducer of mechanical forces for touch sensation in mice. *Nature*, 516(7529), 121–125.

Roza, C., Puel, J.-L., Kress, M., Baron, A., Diochot, S., Lazdunski, M., & Waldmann, R. (2004). Knockout of the ASIC2 channel in mice does not impair cutaneous mechanosensation, visceral mechanonociception and hearing. *The Journal of Physiology*, 558(Pt 2), 659–669.

Schrenk-Siemens, K., Wende, H., Prato, V., Song, K., Rostock, C., Loewer, A., … Siemens, J. (2015). PIEZO2 is required for mechanotransduction in human stem cell-derived touch receptors. *Nature Neuroscience*, 18(1), 10–16.

Sommer, E. W., Kazimierczak, J., & Droz, B. (1985). Neuronal subpopulations in the dorsal root ganglion of the mouse as characterized by combination of ultrastructural and cytochemical features. *Brain Research*, 346, 310–326.

Sommer C., Scha¨fers M., Marziniak M., Toyka K. V. (2001a) Etanercept reduces hyperalgesia in experimental painful neuropathy. J Peripher Nerv Syst 6:67–72.

Sommer C., Lindenlaub T., Teuteberg P., Scha¨fers M., Hartung T., Toyka K. V. (2001b) Anti-TNF-neutralizing antibodies reduce pain-related behavior in two different mouse models of painful mononeuropathy. *Brain Research* 913, 86–89.

Stoll, G., & Muller, H. W. (1999) Nerve injury, axonal degeneration and neural regeneration: Basic insights. *Brain pathology,* 9, 313-325.

Tanga, F. Y., Raghavendra, V. & DeLeo, J. a. (2004). Quantitative real-time RT-PCR assessment of spinal microglial and astrocytic activation markers in a rat model of neuropathic pain. *Neurochemistry International*, 45, 397–407.

Taves, S., Berta, T., Chen, G, Ji, R. R. (2013) Microglia and spinal cord synaptic plasticity in persistent pain. *Neural Plasicity*, 2013-753656.

Tsuda M., Beggs S., Salter M. W., Inoue K. (2013) Microglia and intractable chronic pain. *Glia*, 61, 55–61.

Tsuda M., Inoue K., Salter M. W. (2005). Neuropathic pain and spinal microglia: a big problem from molecules in “small” glia. *Trends in Neurosci*ence, 28, 101–107

Tsuda M., Shigemoto-Mogami Y., Koizumi S., Mizokoshi A., Kohsaka S., Salter M. W., et al. (2003). P2X4 receptors induced in spinal microglia gate tactile allodynia after nerve injury. *Nature* 424, 778–783

von Hehn, C. A., Baron, R., & Woolf, C. J. (2012). Deconstructing the Neuropathic Pain Phenotype to Reveal Neural Mechanisms. *Neuron*, 73(4), 638–652.

Wetzel, C., Hu, J., Riethmacher, D., Benckendorff, A., Harder, L., Eilers, A., … Lewin, G. R. (2007a). A stomatin-domain protein essential for touch sensation in the mouse. *Nature*, 445(7124), 206–209.

Wetzel, C., Hu, J., Riethmacher, D., Benckendorff, A., Harder, L., Eilers, A., … Lewin, G. R. (2007b). A stomatin-domain protein essential for touch sensation in the mouse. *Nature*, 445, 206–209.

Woolf, C. J., & Mannion, R. J. (1999). Neuropathic pain: Aetiology, symptoms, mechanisms, and management. *Lancet*.

Woolf, C. J., Safieh-Garabedian, B., Ma, Q. P., Crilly, P., & Winter, J. (1994). Nerve growth factor contributes to the generation of inflammatory sensory hypersensitivity. *Neuroscience*, 62(2), 327–331.

Xie Y., Zhang J., Petersen M., LaMotte R. H. (1995) Functional changes in dorsal root ganglion cells after chronic nerve constriction in the rat. *Journal of Neurophysiology* 73(5), 1811–1820.